Numerical study of a novel ventilation system added to the structure of a catamaran for different slamming conditions using OpenFOAM

Mobin Masoomi [a], Kourosh Rezanejad [b,*], Amir H. Mosavi [c,d]

[a] Department of Mechanical Engineering, Babol Noshirvani University of Technology, Babol, Iran
[b] Centre for Marine Technology and Ocean Engineering (CENTEC), Instituto Superior Técnico, Universidade de Lisboa, Lisboa, Portugal
[c] John von Neumann Faculty of Informatics, Obuda University, Budapest, Hungary
[d] Ludovika University of Public Service, 1083 Budapest, Hungary

A B S T R A C T

Large-size catamarans' structural behavior is sensitive and critical during the slamming phenomenon. "Ventilation pipes" within the center bow structure are proposed to discharge these cumulative pressure and related loads. The validation case is comprising two different simulation schemes, static and dynamic wedge. First, the appropriate method is chosen based on the accuracy and needed computational running time criteria. The numerical solution approach solves the RANS equation using the Open Field Operation and Manipulation (OpenFOAM) library called "InterFoam and OverInterDyMFoam for static and dynamic mesh respectively. Totally three different impact conditions with four different impact velocities (12 case studies) were considered for the case with added ventilation pipes (amended hull) and the standard model (parent-hull). Apart from the limitation of the proposed plan which is discussed, the results indicate that the recorded pressure and total force decreases by about (15%–50%), and (5%–25%) respectively.

1. Introduction

The increasing demand for faster marine vessels with efficient hulls requires novel platforms, like catamarans, used widely for car transportation, passenger ferries, and military purposes. Catamaran's hull shape is such that the large part of the floated body is under the free surface with a large space between the hull and the free surface; the large deck area causes excellent stability in different sea-state conditions. For higher operational speed, the catamaran would be larger; hence the structural strength would be a critical consideration, especially in the wavy waters and stormy conditions; thus, a comprehensive study needs to perform on the hydrodynamic loads imposed on the catamaran's structure.

The catamarans' slamming is an expanded model of the wedge water entry, which was first investigated by von Karman in 1929 (Von Karman, 1929) by considering the momentum theory and adding mass effect to represent a mathematical model. In 1932 Wagner added the pile-up effects to the basic model, which involved the effect of free surface deformation and curvature near the wall, causing earlier immersion besides decreasing the impact duration; thus, a more accurate

model was obtained (Wagner, 1932). Many researchers expanded these two methods over the following year; Armand and Cointe in 1987 (Cointe and Armand, 1987) and Toyama in 1997 (Toyama, 1996) used the generalized Wagner's theory to investigate the water entry of a cylindrical shape. The Wagner theory involved the pile-up water, but it had a drawback "not considering the spray water." Since then, the spray effects have been added to the theoretical models and numerical solutions. In fact, the spray might cause a reduction of pressure at the edge of the wet surface. The maximum pressure usually occurs around the spray root within the pile-up water, and the pressure is significant from the spray root to the upper spray edge (Yamada et al., 2012).

Some frequently used methods in the hydrodynamic analysis of marine vessels are, Analytical methods, Panel methods (Boundary Element Method (BEM)), Computational Fluid Dynamics (CFD), and Smooth Particle Hydrodynamics (SPH). CFD methods are widely used for slamming issues, particularly complex geometries, and flows. The two main approaches based on this volumetric method are Euler equations regardless of viscosity, Batina (1991); Wendt (2008), and Navier Stokes Equation used for a wide range of problems without any limitation, Mørch et al. (2008); Wang & Guedes Soares (Wang and Soares, 2013). SPH is an advanced meshless method that could predict the

Nomenclature

U	velocity
f_b	body force
p	pressure
T_{vst}	deviatoric viscous stress tensor
S	stress tensor's mean value
U_r	compression velocity
κ	mean curvature for free surface
V	Impact velocity
x	position vector
h	Falling height
g	Gravitational acceleration
c_p	Pressure coefficient
β	Wedge deadrise angle
γ	phase fraction
ρ	fluid density
σ	surface tension coefficient
f_σ	surface tension force
ρ_w	Water density
θ	Roll angle
ω	Pitch angle

α	Yaw angle
t	Time-step
F	Structural Force

Abbreviations

CSF	Continuum Surface Force
RANS	Reynolds Average Navier Stokes
OpenFOAM	Open Field Operation And Manipulation
FVM	finite volume method
CV	Control Volume
CFD	Computational Fluid Dynamic
VOF	Volume Of Fluid
PISO	Pressure Implicit with Splitting of Operator
SIMPLE	Semi-Implicit Method for Pressure-Linked Equation
SWATH	Small Water-plane area Twin-Hull
WPC	Wave-Piercing Catamaran
SPH	Smoothed Particle Hydrodynamics
CBT	Centre Bow Truncation
MRF	Motion Reference Frame
AMI	Arbitrary Mesh Interface
HOS	Higher-Order Spectral
DBIEs	Desingularized Boundary Integral Equations

impact loads more accurately than experimental studies, Oger et al. (2006), and Veen & Gourlay (Veen and Gourlay, 2012).

In 1997, Zhao and Faltinsen (Zhao et al., 1996) used a 2D nonlinear boundary element method to satisfy mass, momentum, and energy conservation equations. Furthermore, they considered that the pressures are small enough in the jet layer zone and can remove from the computations. This method was extended to a three-dimensional problem by Faltinsen and Chezhian in 2005 (Faltinsen and Chezhian, 2005). Most analytical solutions were devoted to symmetry water entry, but Garabedian in 1953 (Garabedian, 1953) and Borge in 1975 (Borg, 1957) expanded the methods to asymmetric water entry problems. In 2004, Wu et al. (2004) represented a method in which the jet layer was added to computation based on a shallow water equation; this method was developed by Xu et al. (2008) for the water entry of asymmetric wedges.

Nair and Bhattacharyya performed a comprehensive study on different axisymmetric objects involving a sphere and two cones entering water using the CFD approach (Nair and Bhattacharyya, 2018a). In 2011, Shahraki et al. (2011) investigated a 2D wedge water entry problem using the SPH method. In 2020, Cheng et al. (2020) studied on bow-flare ship section during the water impact with different roll angles by considering the SPH method. A comparative study of methods' ability (SPH and RANS) was performed in slamming simulation (Sasson et al., 2016). They conclude that both methods could accurately track the pressure and resultant force. A comparative study was performed by Sasson et al. (2016) to evaluate the efficiency of CFD toward the SPH method versus experimental results. They represent that the CFD method showed better compatibility with experimental results.

Several simplified models introduce by researchers Howison et al. (1991), Fraenkel and McLeod (1997), and Mei et al. (1999) to eliminate the complexity of the water entry problems. In 1987, Greenhow added the influence of gravity to the analytical model (Greenhow, 1987) and observed that the consideration of gravity could be ignored, except for the jet spray zone. In 1999, for further investigation of the simplified approaches, the effect of considering the viscosity studied by Muzafreija et al. (Muzaferija, 1999), they concluded that, although the viscosity could be an effective factor in predicting the free surface variations, the values for hydrodynamic forces approximately match with the inviscid model. In 1997 and 1998, Korobkin and Campana studied compressible fluid for water entry problems (Korobkin, 1996) and (Campana et al., 2000); before, water was considered incompressible.

Most investigations related to impact loads due to slamming have been done based on monohull vessels like Kapsenberg (1947), Luo & Soares (Luo and Soares, 2012). Still, some investigations performed in recent years based on a multi-hull; in 2020, Sun et al. (2020) numerically investigated the slamming loads imposed on the trimaran with different impact conditions such as mass, velocity, etc., considering the CFD simulations. Zong et al. (2020) did an experimental test on the water entry phenomenon of a trimaran ship section. Besides the CFD solution or practical tests, some researchers like Tang et al. (2020) simulated the trimaran motion and wave imposed load such as slamming by considering a novel nonlinear three-dimensional time-domain Rankine-Green matching method. In 2021 Almallah et al. (2021) used a full-scale wave-piercing catamaran (INCAT 89 m) encounter with waves by considering the CFD method, and Shabani et al. (2019) investigated another aspect of these catamarans, center-bow length, and specifications. They conclude that the slamming loads increase with a bigger center-bow length.

There is a phenomenon in water entry problems that is related to air, aerated, and non-aerated cases, as Mai et al. (2019) experimentally investigate this criterion for free falling off a rigid flat plate. They concluded that the aeration process could significantly decrease the impact load due to lowering the air pressure and water surface distortion. Oh et al. (2009) also conducted a further investigation on the generation of air pockets during the water entry of a flat bottom box-type model. In addition to the experimental tests, many numerical solutions were performed for the air-related phenomenon at water entry such as Truong et al. (2022) who analyzed a fluid-structure interaction approach of a flat stiffened plate to assess the influence of air cushion for a small angle of impact. O'Conner et al. (O'Connor et al., 2022) studied the air pocket phenomenon for water entry of a flat plate to assess the effects of geometric parameters such as area, depth, and volume on the response of slamming pressure and force under different impacts velocities.

Another critical factor related to water entry problems is the structural loads. Swidan et al. (2016) did both experimental tests and numerical solutions to estimate the actual force imposed on the structure toward the impact velocity. Xie et al. (2020) added structural analysis based on pressure loads that are extracted from CFD solution (Fluent Software) to predict the strength of the Ultra-large Container Ship (ULCS) under different slamming conditions. Furthermore, in 2021, Lin

et al. (2021) used the commercial software STAR CCM + besides considering the experimental test to investigate the slamming loads and pressures induced on a 10,000 TEU container ship encounter with waves. They concluded that, as the wavelength increased, the slamming pressure could decrease only for asymmetric (with rolling angle) impact.

So far, many research activities have been presented focused on the slamming phenomenon and discussed hydrodynamic and structural methods for a wide range of simple geometries or complicated bodies such as marine vessels. Little research studies have been performed on the slamming of two-hull vessels. A significant research gap exists for the air pressure and air-cushion phenomenon between the two hulls and free surface, considering their effect on the hydrodynamic parameters and as well as structural loads. In the present paper, an innovative idea is proposed for the first time to affect the air cushion and air compression. The proposed idea behind the present research is based on implementing the air ventilation pipes within the deck structure to transfer the extra compressed air. First, these pipe groups are designed and added to the standard catamarans' hull; second, this cumulative system numerically analyzes using OpenFOAM's solvers in different impact conditions compared to the standard catamaran. These ventilation pipes have not been used in marine vessels.

2. Material and methods

The slamming phenomenon is an issue in water entry problems; the water entry is complex and nonlinear, with water pile-up, water spray, water jet, and generating air bubbles beside air entrapment areas. The air bubble or air pockets are phenomena occurring for critical impact conditions; the point is, they only cause cavitation, noise, or small oscillation in pressure value after the impact. Although these physical phenomena are critical in some cases, the most striking aspect is the "slamming force." The structural response of marine vessels is more akin to slamming forces and structural strength.

In the present study OpenFOAM which is the first generated software based on the c^{++} language for continuum mechanics problems is used as the numerical solver of water entry problems. Open-source licensing software comes with many standard or extended libraries and solvers. Depending on the requirements, the users can transform them into in-house codes or add extra features to standard solvers, InterFoam is selected from the incompressible multi-phase library to simulate the water entry problem; this solver is based on the Finite Volume Method (FVM) and RANS equation. Three different falling water entries, 3D wedge, cylinder, ship section, and slender circular cylinder, were investigated with OpenFOAM libraries by Wang et al., in 2021 (Wang et al., 2021).

The CFD involved some partial differential equations discretized into the system of algebraic equations to be solved. This process needs two main discretizations; the first is domain discretizations, and the second is for the equations (Hirsch, 1991), (Patankar, 2018). FVM is a solution for the domain discretization scheme generating the computational domain and involves the point's position and the boundary description. The whole domain is divided into small volumes called Control Volume (CV) or control cells. These Control volumes are general polyhedrons involving multiple boundaries and internal faces. Boundary faces are related to faces near the domain boundaries, and inner or interrelated faces imply the correlation between the control volumes. A further discussion on FVM and applications is mentioned in Versteeg and Malalasekera (2007) and Ferziger and Peric (Ferziger et al., 2002).

2.1. Governing equation

InterFoam is a two-phase solver of the standard library of Open-FOAM used in the present study; the method by which the multi-phase problems simulate is Volume Of Fluid (VOF), first presented by Hirt & Nichols (Hirt and Nichols, 1981). The basic idea is to use the indicator function to recognize the syntax of each cell with each fluid. Thus, a new sort of equation needs for the continuity and momentum equations:

$$\nabla . U = 0 \tag{1}$$

$$\frac{\partial \gamma}{\partial t} + \nabla . (U\gamma) = 0 \tag{2}$$

$$\frac{\partial(\rho U)}{\partial t} + \nabla . (\rho U U) = -\nabla p + \nabla \cdot T_{vst} + \rho f_b \tag{3}$$

where U is the field related to the Velocity, γ represents the phase fraction, f_b, body force, ρ is the fluid density, and p is the pressure. The only remaining variable is T_{vst}, deviatoric viscous stress tensor, described as below:

$$T_{vst} = 2\mu S - \frac{2\mu \ (\nabla \cdot U)I}{3} \tag{4}$$

$$S = \frac{\left[\nabla U + (\nabla U)^T\right]}{2} \tag{5}$$

where S denotes the stress tensor's mean value, representing the Kronecker delta, and μ is the fluid kinematic viscosity. As before said γ is the phase fraction which is $\gamma = 0$ for the gas (air) and $\gamma = 1$ for the liquid (water), and the syntax phase fraction occurs at the interface boundary. Now it is the turn to change the physical properties by considering the weighted averages value based on the phase fraction values, as described below:

$$\rho = \rho_L \gamma + \rho_g (1 - \gamma) \tag{6}$$

$$\mu = \mu_L \gamma + \mu_g (1 - \gamma) \tag{7}$$

The subscript L and g are related to liquid and gas, respectively. The most striking issue is ensuring boundedness besides conservativeness of the phase fraction, especially at the interface and high-density flow rates. A slight misunderstanding in cell volume fraction may significantly decrease the method's accuracy. The surface tension and related pressure gradient must evaluate correctly to track the free surface and movement accurately; this needs a high-resolution griding scheme in the free-surface areas. A further discussion in this field is mentioned in (Berberović et al., 2009); in the present study, a phase fraction method is an advanced approach represented by Open-CFD Ltd, VOF, in the framework of the FVM method. In this method, the related equations to phase fractions solves distinctly, as mentioned below:

$$\frac{\partial \gamma}{\partial t} + \nabla \cdot (U_L \gamma) = 0 \tag{8}$$

$$\frac{\partial(1 - \gamma)}{\partial t} + \nabla \cdot \left[U_g(1 - \gamma)\right] = 0 \tag{9}$$

To represent the new form of equation (8), a further designation is needed, U in equation (10), which is a weighted average effective velocity (Damián et al., 2012), and U_r, the vector form of the relative velocity, called: compression velocity. Now by substituting these variables, the new form is described below:

$$U = \gamma U_L + (1 - \gamma)U_g \tag{10}$$

$$U_r = U_L - U_g \tag{11}$$

$$\frac{\partial \gamma}{\partial t} + \nabla \cdot (U\gamma) + \nabla \cdot [U_r \gamma (1 - \gamma)] = 0 \tag{12}$$

As mentioned above, an additional convective term is added to the equation is, U_r. This value's function compresses the free surface into a more precise and sharper one. Albeit the compression is only the name and has not physically occurred for this variable, this term only affects the region within the free surface as an artificial donation to phase fraction convection. This value vanished for the cells outside of the free

surface. The two-phase problem is considered with an interface and a newly generated additional force, "surface tension." Due to the pressure gradient at the two-phase intersection, this force assesses with Continuum Surface Force (CSF) (Berberović et al., 2009). This value is a parameter added to the momentum equation, Eqn (2).

$$f_\sigma = \sigma \kappa \nabla \gamma \tag{13}$$

$$\kappa = -\nabla \cdot \left(\frac{\nabla \gamma}{|\nabla \gamma|} \right) \tag{14}$$

where σ is the surface tension coefficient, κ is the mean curvature for the free surface, and f_σ is the surface tension force. Since the fluids are considered Newtonian and incompressible ($\nabla.U = 0$), the linear correlation is dominant for stress and strain tensor. This caused the more accessible discretization approach represented below:

$$\nabla \cdot T = \mu \left[\nabla U + (\nabla U)^T \right] = \nabla \cdot (\mu \nabla U) + (\nabla U) \cdot \nabla \mu \tag{15}$$

$$p_d = p - \rho g \cdot x \tag{16}$$

The pressure gradient, p_d, the gradient between the body force and additional density gradients at a particular position, x denotes the position vector. By substituting the above considerations, Eqn's, (13), (15), (16) in the momentum equation, a simplified relation for a two-phase problem is as below:

$$\frac{\rho U}{\partial t} + \nabla \cdot (\rho U U) - \nabla \cdot (\mu \nabla U) - (\nabla U) \cdot \nabla \gamma = -\nabla P_d - g \cdot x \nabla \rho + \sigma \kappa \nabla \gamma \tag{17}$$

2.2. Numerical set-up

Two different approaches to the slamming load evaluation are; the seakeeping tests involve a complete model of the vessel encountering waves in a wave tank. These tests broadly consist of local and global loads at any direction; French et al. (2015); He et al. (2013); Lavroff et al. (2011); Thomas et al. (2011) are among researchers who performed seakeeping tests. The drawback of using this model is the model set-up complexity with the high cost and time-consuming.

The second is the drop test technique, a widespread and repetitive test case, especially for slamming load calculation. All the water entry cases could test experimentally with this method, including wedge impact, cylinder impact, ships' bow segment impact, and lifeboats impact to water, are examples of this approach's applicability. Although there were many simulated cases with this method, multi-hull vessels like a catamaran were not discussed so much and needed further investigations on such a marine vessel. In 2004, Whelan (2004) performed various drop tests for a 2D cross-section of seven catamaran models. The drawback of the method was that the recorded slamming force values were bigger than real or 3D cases, thoroughly discussed in Davis & Whelan (Davis and Whelan, 2007).

As mentioned earlier, the drop tests use for the slamming phenomenon; thus, in the present study, a numerical tank based on the experiments performed by Barjesteh et al. (Barjasteh et al., 2016) is considered. The framework of the numerical solution is InterFoam from the OpenFOAM library package; InterFoam is a solver appropriate for multi-phase problems based on the RANS equation and the VOF scheme. The overall strategy for verifying the present method is the comparison of the results for a wide range of impact conditions, which inherently prove the method's proficiency and stability. Some investigations put their concentration on assessing the different methods in-use for temporal or spatial accuracy of OpenFOAM for different case studies, such as Lee (2017) performed a comprehensive study to analyze the discretized formulation of NS (Navier stokes) equations, and test the temporal accuracy related to time integration schemes, and introduced a simple but efficient method to track the volume flux with 2nd accuracy.

Both approaches (2D and 3D) are simulated by the same numerical

configuration with different griding schemes and some differences in boundary and initial conditions. The underlying strategy of pressure and velocity coupling is PIMPLE, a combination of Pressure Implicit with Splitting of Operator (PISO) and Semi-Implicit Method for Pressure-Linked Equation (SIMPLE). An important factor is the "momentum predictor" which is set to "no" in order to predict the velocity based on former sources instead of using former pressure. The total approach of the present method is Implicit which is more stable as well as needs more computational time and costs. The implemented temporal discretization scheme is, Crank-Nicolson with a blending factor, ψ, that is equal to ψ = 0.5 to gain the benefits of both Euler schemes (ψ = 0, robust but first-order accurate), and pure Crank- Nicolson (ψ = 1, accurate but oscillatory, second-order accuracy).

As represented in (Johannessen, 2012), the effect of the turbulent regime is negligible for the impact phenomenon. The shortness of the impacting time causes rapid changes in the high-pressure points and values (in milliseconds); thus, there is no time for the influence of diffusion terms, but we in the present paper used the K-ω SST to close our results realistically. The maximum pressure usually occurs around the spray root within the pile-up water, and the pressure decreases from the spray root to the upper spray edge. Although the spray effects on the maximum pressure are not significant, the present method tracked this phenomenon using high-quality mesh around the wedge.

The primary step of each numerical is setting the appropriate initial and boundary conditions, the two-phase problem with a fixed velocity of water entering from the bottom of the domain needs special boundary conditions which are illustrated in Fig. 1 for both pressure and velocity. The Pressure Inlet & Outlet Velocity boundary condition prevents the sudden increase in air pressure for the top boundaries, and the distance between the wedge apex and free surface is undependable to falling height.

The tank dimensions can affect the output pressure; thus, the selected dimensions are L = 1.22 m, H = 0.671 m, Fig. 1, as used in the experimental study. The tank dimensions could have a discernible effect on the pressure and force imposed on the structure, especially for 2D cases; as concluded in Agard (Aagaard, 2013), the small domain could increase the force or pressure by about 30% rather than a very large domain. The Flow Rate Inlet Velocity boundary considers simulating the water entrance for the bottom of the domain.

2.2.1. Mesh convergence analysis

As indicated in the previous section, there were two choices of impact approach, static wedge or dynamic wedge, in the present study static approach is more reasonable and elaborated as a basic approach for the rest of the simulations. The two standard pre-processing tools in OpenFOAM which help the users generate the mesh are, BlockMesh, SnappyHexmesh, and TopoSetDict. The griding scheme is shaped by rectangular and hexagonal cells generated by BlockMesh and the multi-subset domain built by TopoSetDict in three different zones, in which
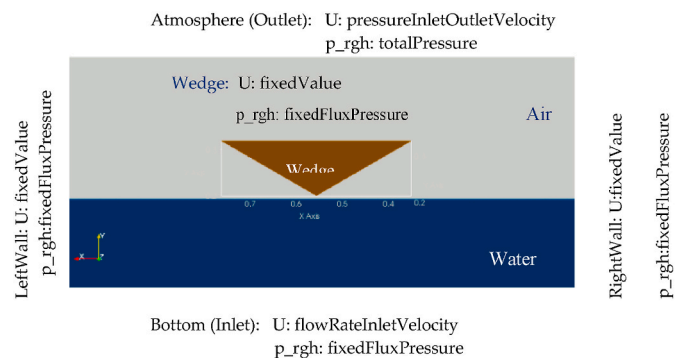

Fig. 1. The overall information of boundary condition and initial volume fraction of wedge (β = 30°).

the cell size is halved at each sequence zones. Maximum instantaneous pressure is the most critical value, most attention is engaged in it therefore in the case of the mesh independence study maximum pressure plays a major role. According to this, as in the previous section mentioned, an experimental test (Barjasteh et al., 2016), which is a comprehensive study in wedge water impact choose for further investigation. The case is, a wedge (β = 30°) and h = 0.5 m (falling height) by considering different griding strategies shown in Table 1. The local snapshots of the griding size are also represented for all mesh types in Fig. 2.

As shown in Fig. 3, Four different griding strategies cover all borders of the problem in the mesh convergence analysis. G-1, G-2, and G-3 are the three hypothesises pressure transducer that is allocated based on the experimental test. The results indicate that the calculated pressure for medium-quality and high-quality grids are almost the same, p = 35,420, 35,685 [pa] of G-1 versus p = 38,222 [pa] of experimental results (Barjasteh et al., 2016). Almost E = 6.5% recorded for error in maximum pressure value against experiment and less than E = 0.5% differences between medium and high-quality mesh observed. Although overall simulation time, Time = 8, 1, 0.8, 0.5 h the recorded estimated time for four case studies, there is a point here, these cases were 2D and the rest of the simulation consists of a 3D simulation of the bow section. Due to the sensitivity of the impact phenomenon relative to time and location, it is more reasonable to choose medium-quality as a reference grid size with enough accuracy and lower computational running time.

Although the PIMPLE solver has the option to limit the time step to a maximum CFL number, thus the solver automatically chooses an appropriate time step Holzmann (2016), the fixed time step could also be used. In this part, like the mesh convergence study, the water entry problem considered for the wedge (β = 30°) for four different fixed time steps (not adjustable run time) to evaluate the effects of different time steps, Table 2. In fact, the solver could not change the time steps automatically. As could be inferred from Table 2, and Fig. 4, case (IV) represents the most efficient and accurate among all time steps, needless to say, too small time step (case (I)) as well as too big (case (V)) impose more computational costs and uncertainties to the numerical solution.

As claimed, the related results of adjustable run time, maximum peak pressure p = 35,685 [pa] as well as execution time, t = 1-h show better compatibility with the experimental result. This utility helps the solution stability, especially for 3D case studies as well as complex grids. The maximum courant number set; (Max Co = 0.5) could result in a more stable simulation, especially for 3D and a more complicated griding scheme.

In the case of interface compression, which is a phenomenon that put significant alteration in final results especially in cases with a sharp interface in a period such as a wave generation (Afshar, 2010), and in a lower level of importance for a case like water entry problems. A possible solution that is elaborated in OpenFOAM is introducing an extra term, Artificial Compression to the equation of phase fraction convection, as previously mentioned in equation (12). This compression factor could impose an artificial pressure on the interface to avoid dispersion or dispersing, Brief physical explanation. The parameter which is used to control the artificial compression is "cAlpha," a zero value, which means: compression velocity and pressure, and devoting higher numbers imposes a variety of artificial compression at the interface.

In this section, we investigate the total influence of different values

of "cAlpha," on maximum pressure recorded at pre-defined pressure gauges (G-1), the same as the mesh convergence study, a wedge (β = 30°) and h = 0.5 m (falling height) by considering different values of cAlpha. Totally cAlpha = 0 means, removing convective compression and eliminating the compression velocities, consequences the alpha (phase fraction) changed to a diffusive condition. Generally, the cAlpha is considered as cAlpha = 1 in most case studies.

As predicted, the most efficient artificial compression is cAlpha = 1 which could accurately predict both the maximum pressure (about p = 37 [kpa]) as well as the occurrence point (almost in t = 0.0046 s), Fig. 5. The results for other values did not satisfy our case needed accuracy. For further explanation, simple contours consist cAlpha = 0, 1, and 2 are illustrated in Fig. 6 the interface loses its sharpness at cAlpha = 0 which causes misprediction of pressure immensely. For the case cAlpha = 1.5, as illustrated in Fig. 5, the maximum pressure value is similar to cAlpha = 1 (almost p = 35 [kpa]) with a difference, the occurrence time of peak pressure moved to t = 0.005 s.

2.2.2. The water entry approach (dynamic mesh/static mesh)

There were two choices for water entry problems, static wedge, and dynamic wedge, that were previously investigated by Nair and Bhatta-charyya (2018b) in 2018, albeit using dynamic wedge was usual before, but the idea of using fixed wedge was proposed formerly by Masoomi et al. (2017) in 2017. Doustdar and Kazemi in 2019 (Doustdar and Kazemi, 2019) compared the fixed and dynamic methods for the simulation of stepped planning craft by considering the STAR CCM for the dynamic mesh (overset mesh technique) and ANSYS CFX CFD toolboxes for the static approach. They conclude that each method has its own advantages, and both methods could accurately simulate the solution compared with experimental results. In fact, each method (static/dynamic), Fig. 7, has its advantage or disadvantage, static-mesh is more efficient in terms of time and computational power saving, but the dynamic mesh is more similar to the experimental test cases with more diagram adaption. These two methods should be used and verified with experiment to make a reasonable decision.

A comprehensive investigation of the momentum and gravity effect for a fixed wedge with a constant water inlet was performed by Clarkea and Tveitnesb in 2007 (Fairlie-Clarke and Tveitnes, 2008). The cumulative force imposed on the wedge is a summation of flow momentum, gravity, and added mass momentum; the added mass force is more effective than others; thus, it is reasonable to track the added mass changes for a fixed wedge. The variables are different since there are two modes for the water impact problems: dry-chine and wet-chine. They conclude that based on the added mass coefficient for dry chine (c_{my}) and wet chine (c_{mb}), equations 18 and 19, since (c_{my}) only depend on the deadrise angle, the added mass is constant during the dry-chine mode, and whatever the water proceeds to the top of the wedge and the wedge immersed into water (wet-chine), the added mass increases with a gentle slope (c_{mb}). Dry chine is the only mode considered in the present study; the added mass assumes a constant value; accordingly, it is inferred that fixed wedge and dynamic wedge are the same, particularly for dry-chine impact mode.

$$c_{my} = \frac{\pi}{2} \left\{ 0.15 + \frac{0.85}{\cos(\beta)} \left(1 - \frac{2\beta}{\pi}\right)^3 \right\} \qquad (18)$$

$$c_{mb} = \frac{\text{added mass}}{\rho \left(\frac{\pi}{2}\right) \left(\frac{\beta}{2}\right)^2} \qquad (19)$$

Moving-wedge: different dynamic motion strategies used at OpenFOAM are; MRF (Motion Reference Frame), AMI (Arbitrary Mesh Interface), OverSetMesh, and finally, the simplest one is the mesh moving approach. Each method's applicability is appropriate for related cases; MRF is efficient for cases with a dynamic domain such as the sloshing in the tanks. AMI is a kind of dynamic mesh in which a
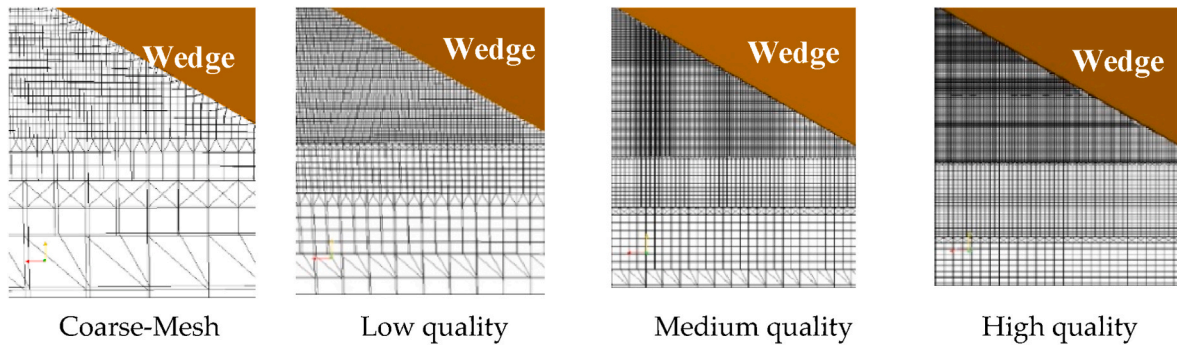
Table 1
Different grid sizes for grid convergence study.

Mesh-type	Coarse-mesh	Low-quality	Medium-quality	High-quality
Basic-grid	(0.05, 0.01 , 0.055)	(0.02, 0.004 , 0.022)	(0.0125, 0.002 , 0.014)	(0.01, 0.00625, 0.001)
Number of cells	4189	26112	66556	183363

Fig. 2. The Figure of a detailed griding scheme for the wedge, deadrise angle ($\beta = 30°$).
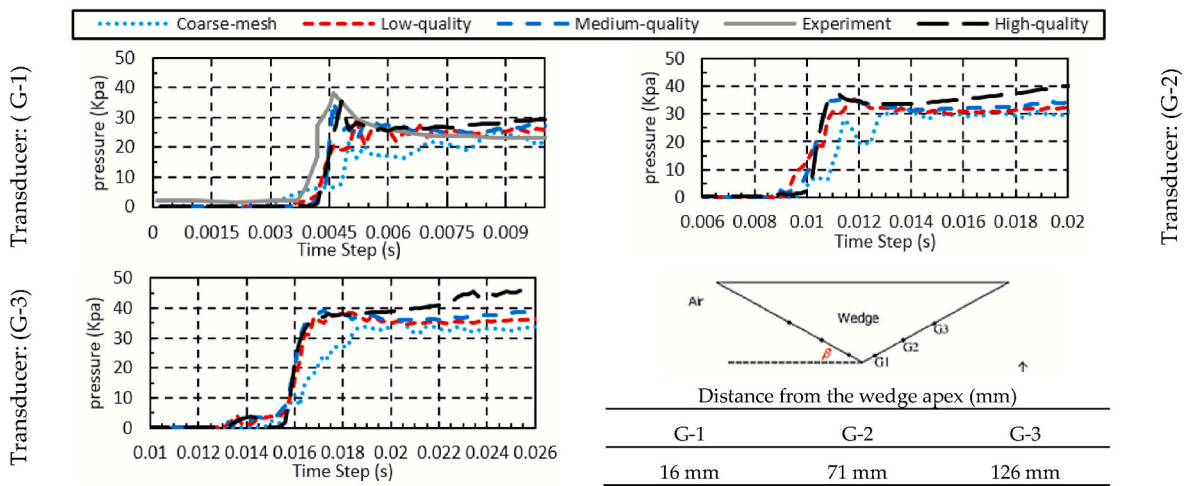

Fig. 3. Mesh convergence analysis based on maximum pressure for four different griding schemes.

Table 2
Different time steps for water entry of the wedge ($\beta = 30°$), h = 0.5 m

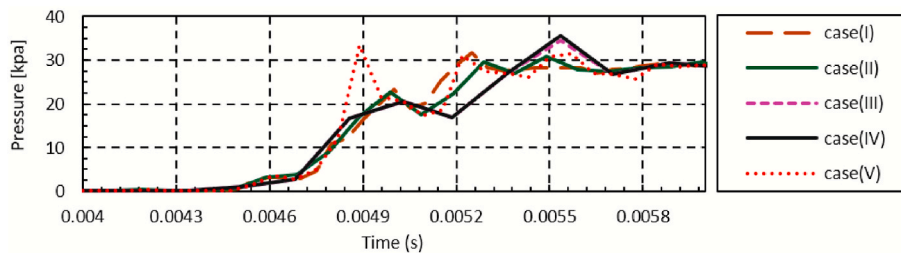| Case. Num	I	II	III	IV	V	Adjustable Run time	Experiment
Time-step	1e -5	2e-5	8e-5	1.6e-4	3.2e-4	-	-
Execution time	7500 (s)	4850 (s)	2876 (s)	2850 (S)	3313 (s)	3510 (s)	-
	2.1 (h)	1.34 (h)	0.8 (h)	0.8 (h)	0.92 (h)	1 (h)	-
G-1(max. Pressure)	31640 [pa]	32620 [pa]	34510 [pa]	35400 [pa]	33500 [pa]	35685 [pa]	38222 [pa]

Fig. 4. Time step analysis based on maximum pressure for five different time steps.

particular zone slides on adjacent cells; this type is recommended for rotary motions like marine propellers, Masoomi and Mosavi (2021), turbine blades, Nuernberg and Tao (2018), and Hidalgo (2021). Finally, the OverSetMesh is a highly efficient method with unlimited motions in all directions for most cases. This approach is based on FVM discretization by considering two zones, one is around the body (front mesh), and the other is the domain zone (background mesh); these two zones relate to each other. Since the falling height is large in the verification case, h = 0.75 m, the overset mesh is selected to cope with this simulation. Cell types divide into three sets, as shown in Fig. 8.

Hole cells: included the cells in which no calculation usually involves the dynamic body; hole cells are the wedge in the present paper.
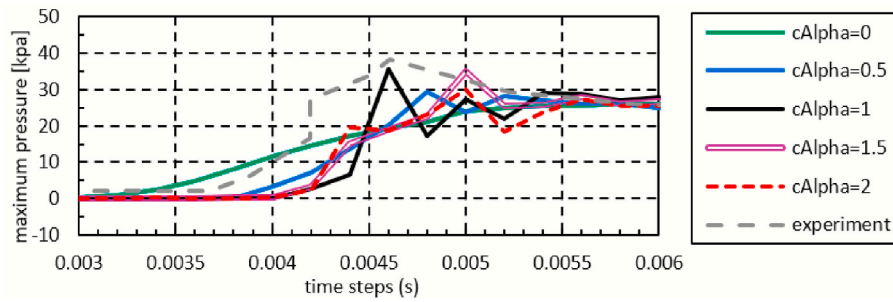
Fig. 5. The variations of the relative maximum recorded pressure by considering different artificial compression "cAlpha" for a 2D wedge impact.
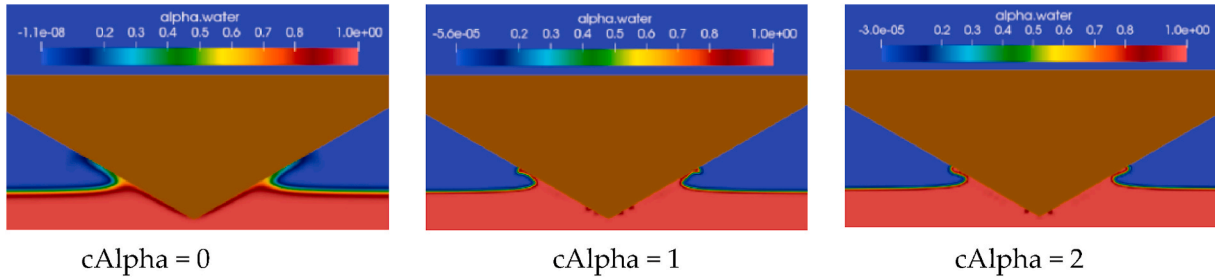

cAlpha = 0   cAlpha = 1   cAlpha = 2

Fig. 6. The contour view of VOF by considering different artificial compression "cAlpha" for a 2D wedge impact.

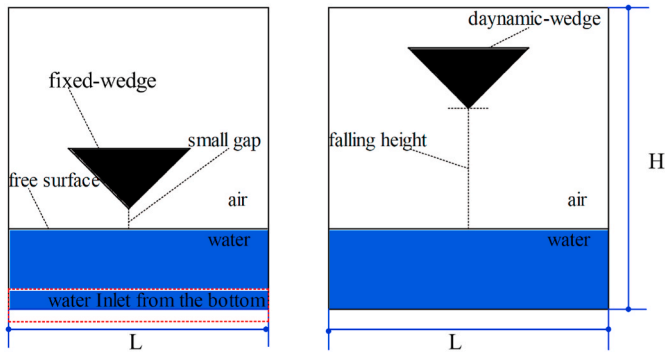**Fig. 7.** A schematic view for the wedge impact simulation for static and dynamic mesh.

- Acceptor Cells: these cells are the boundary of background mesh and OverSetMesh that performs the interpolation process between two zones. These cells are only hypothetical cells, and no discretization equations solve.
- Donor Cells: these cells are adjacent to acceptor cells that fill the gap in the number of the variables and equations by considering the interpolation equation at acceptor cell centers (Gopalan et al., 2015).

Fixed-wedge: the wedge fixed at the location and the water flow inlets from the bottom of the domain with constant velocity obtained from equation (20). a small gap deems to be a steady state at the impact from the start point.

$$v^2 - v_0^2 = 2gh \tag{20}$$

where "V" is the impact velocity, "V_0" is the primary speed considered zero, "h" is the falling height, and g is the gravitational acceleration. The simulations were performed individually for a fixed wedge (InterFoam solver) and dynamic wedge (OverInterDyMFoam solver) with the same mesh quality. Both models verify with different impact conditions; Fig. 9
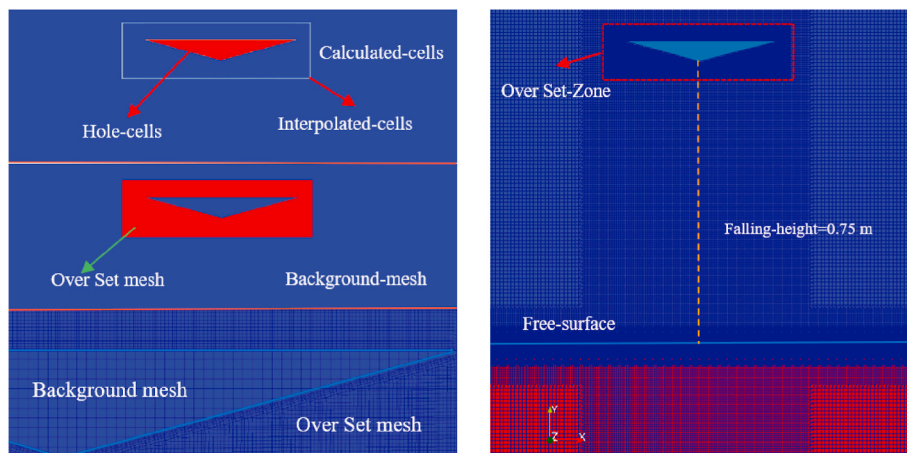

Fig. 8. Cell types and ZoneID for the wedge ($\beta = 15°$) and falling height = 0.75 [m] test case.

a) Wedge ($\beta = 25°$)- falling height (0.2 m)   b) Wedge ($\beta = 15°$)- falling height (0.75 m)
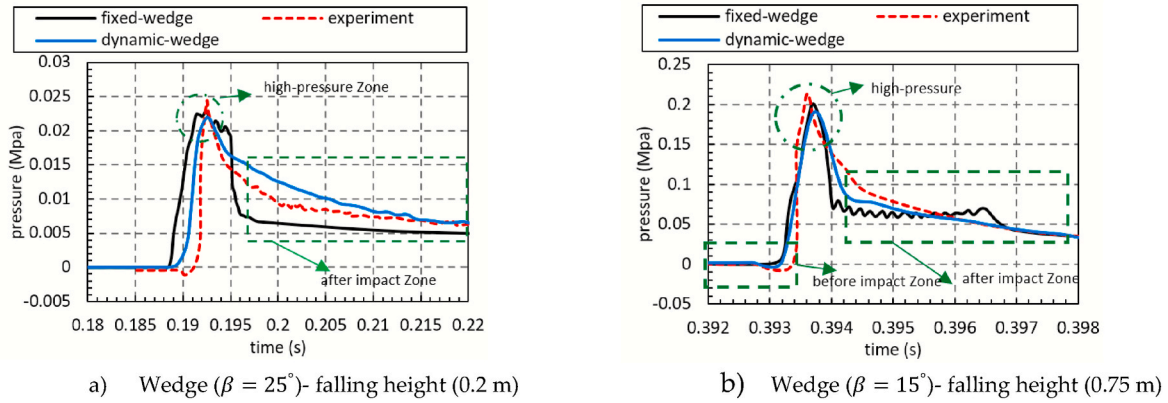
Fig. 9. Comparing pressure for fixed and dynamic wedges at different impact zone, cases (a), (b).

shows the maximum pressure for two states, wedge ($\beta = 25°$, $15°$) and falling height h = 0.2, 0.75 m, respectively; this selection is to test the models in the most critical impact conditions. As shown in Fig. 9, three different impact zone could be devoted to the diagram, before and after the impact zone and the high-pressure zone; a key point here is the high-pressure zone which is essential for the designing process.

As could be inferred, the results for the three cases are almost similar. Still, the recorded pressure is higher for fixed wedges than others by eliminating the reduced acceleration. For further comparison of the two methods, the velocity and pressure variations are in graphs, Fig. 10. For the dynamic wedge approach, the critical parameter (the velocity) is almost the same as the fixed wedge (constant inlet water velocity); thus, for the impact zone, the impact velocity for the static and dynamic wedge is almost constant with a negligible difference.

The reason for using these two cases (a and b), Fig. 9, is to evaluate the reliability of the method for minimum and maximum pressure of the fixed-wedge, dynamic-wedge, and experiment results. As shown in Fig. 9, the pressure values oscillate for the fixed wedge after the impact zone. This phenomenon occurs because of neglecting the body's deceleration during the dry chine in fixed-wedge simulation. Although this simplification is not affecting the result, the point is the difference in velocity, just about 0.1 m/s, caused some extra air pockets near the wedge boundaries. As the impact velocity is faster or the deadrise angle is smaller, these phenomena become more visible. Topliss et al. (1993) investigated the effect of air pockets on the pressure oscillation during the wave impact on vertical walls; they concluded that the recorded pressure oscillations are due to the vibrations of air-filled gas bubbles. These values are small compared to peak pressure; therefore, their effects are more obvious only when the pressure is low (after impact region).

Table 3
Final results and error percentage for three different approaches, static/dynamic wedge, experimental tests.

Method	$\beta= 25°$, h = 0.2 m	Error [%]	$\beta= 15°$, h = 0.75 m	Error [%]
Fixed-wedge	22560 [pa]	7.71%	192520 [pa]	10%
Dynamic-wedge	21970 [pa]	10.1%	189560 [pa]	11.4%
experiment	24447[pa]	0	214000 [pa]	0

As could be inferred from Table 3, the maximum error is E = 11.4% for the worst impact condition; the average error for such cases is up to E = 30% error, particularly for small deadrise angles (Nikfarjam et al., 2019). According to Fig. 9, why is the peak pressure for a fixed wedge higher than for a dynamic wedge with the same solver and boundary condition? The answer is "impact velocity," for a fixed wedge, the velocity is constant; for a dynamic wedge, the velocity has a slight decrease (about $\Delta V = -0.1$ m/s); this could change the impulse pressure by about 1 or 2%, Fig. 10.

The final question is, why are static simulations chosen when the dynamic approach is reachable? The answer is computational power; since tracking the peak-pressure values is highly dependent on the mesh resolution, explained in the next section, section 2.2.2, it is reasonable to use the cases with higher mesh quality. In the present study, the bow section of the catamaran simulates under different impact conditions (At least 12 case studies). Thus, using a dynamic approach is time-consuming, which will have a discernible effect on selecting mesh resolution and total solution time. The final decision is that: using a static method for a water entry of an extensive and complicated body like an INCAT catamaran caused high accuracy and low computational cost for
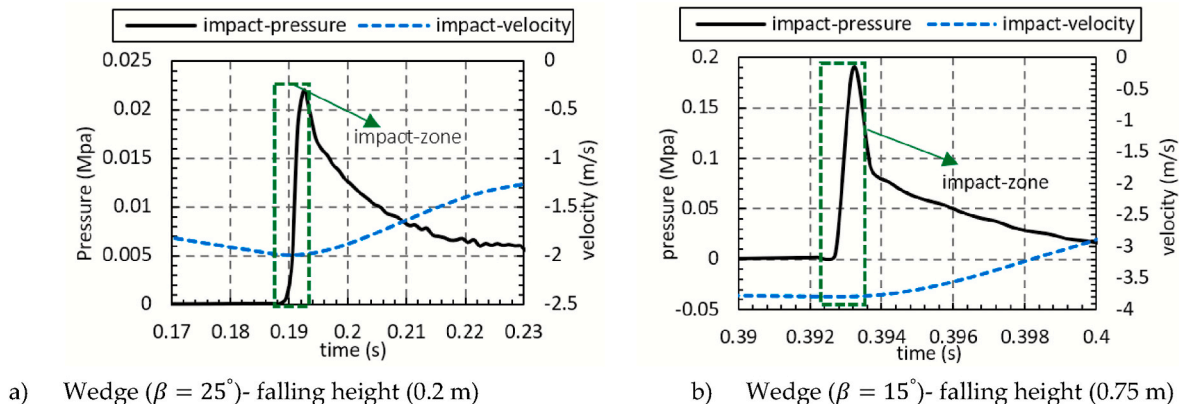

a) Wedge ($\beta = 25°$)- falling height (0.2 m)   b) Wedge ($\beta = 15°$)- falling height (0.75 m)

Fig. 10. Comparing impact pressure and velocity for cases (a), (b).

the rest of the simulation.

On the other hand, the main aim of using the OverSet mesh technique was only implementing the dynamic wedge impact to compare the pressure between static and dynamic water entry problems. As mentioned, the static mesh approach could accurately simulate this problem thus, the only method used for the catamaran was the static mesh approach to decrease the computational cost. In fact, the dynamic approach (with the OverSetMesh technique) would not be considered for catamaran water entry case studies.

2.2.3. Verification study

So far, the overall simulation aspects are addressed such as the numerical setup, boundary conditions, appropriate griding scheme, and the overall movements (dynamic or static mesh). In this section, all simulations are performed based on an approach that is proved in the previous sections. The most important part of each numerical solution is verifying the results toward experimental or other valid whether numerical or theoretical solutions. In the present study, this process is performed for two cases to prove the high fidelity of our solution. Although a 2D wedge impact verification is comprehensive and sufficient, as most numerical solutions of the water entry problems are verified based on it, a further verification case is also provided exactly based on the 3D case of the INCAT bow section to assess the method's accuracy in detail. A comprehensive study performed for the 2D wedge involved all impact conditions as tested in experiments, (Barjasteh et al., 2016). Thus present verification departs into two parts, 2D wedge impact, and 3D Bow section impact based on two criteria: pressure coefficient (c_p) and the maximum pressure (p_{max}) respectively.

2.2.3.1. 2D wedge impact verification.

A wedge impact is a standard verification test for water entry problems, 3D for experimental tests, and 2D in most numerical solution approaches. In most references, the simulations were performed for various impact conditions to better assess their numerical approaches. For this, five different case studies are used, as shown in Table 4. Actually, we need to investigate the model's accuracy for a wide range of wedge deadrise angles with a constant falling height, h = 0.5 m. The main criterion to compare the results is the maximum pressure coefficient $(C_p)_{max}$ which is calculated based on the maximum pressure extracted by the present numerical solution, the related equation is:

$$(C_p)_{max} = \frac{P_{max}}{0.5\rho_w \cdot V^2} \tag{21}$$

Where" p_{max} " is the maximum pressure recorded, c_p is the pressure coefficient, ρ_w represents the water density, and "V" denotes the velocity of inlet water at impact time.

The initial setting for all five cases is similar, apart from the wedge's geometry. Since the verification study is based on the 2D case with medium-quality mesh (0.0125, 0.002, 0.014) for all cases, the simulation running times were equal, just about h = 2 h. To better understand the pressure distribution and the water-related phenomenon, pile up, jet layer, and free surface variations, for instance, sequential time steps are represented, t = 0.006 s, 0.012 s, 0.02 s, 0.03 s, Fig. 11, by considering all case studies in a diagram and comparing them with former experimental and theoretical results in an integrated diagram, Fig. 12, the maximum pressure for each case is calculated at the hypothetical transducer point in the middle of the wedges wing. It could be concluded that, although the solution is accurate for bigger deadrise angles, "β >

20°," less than E = 5% error, for smaller angles "β < 20°" The numerical solution loses its reliabilities, considering the results from Fig. 12.

As represented in (Nikfarjam et al., 2019), the results' accuracy is highly dependent on the deadrise angle, such that, for the wedge β = 15° the discrepancy between experimental and numerical results is about E = 29%, and for the larger angle of impact, the difference became smaller; the same conclusion was reported by Shah et al. (2015). The runaway water in slamming is divided into two-part: raised water (pile-up) and a jet spray, that; Pansiroli and Shams mentioned that 60%–80% of the impact energy is devoted to "risen water." (Panciroli et al., 2015). When water impacts a wedge with a bigger deadrise angle, the wetted wings' wedge length decreases; thus, the water rises quickly along with the wedge besides boring lower pressure values. Therefore, the impact pressure decreases for the bigger deadrise angles due to changes in the pile-up coefficient and the wetting length of wedges' bodies.

2.2.3.2. 3D bow section impact verification.

For the second validation case study, a 3D bow section of an INCAT catamaran is considered based on Swidan et al. (2017). The bow segment of the vessel is considered to simulate the slamming phenomenon; the overall characteristics are mentioned in Table 5. As said in the previous sections, a similar method is used for the wedge water entry of the bow slamming of the INCAT catamaran. Although the experimental study was performed for different impact velocities, the validation performed for both $V_{impact} = 4$, 5 m/s due to validate the present numerical method for the worst impact condition. Five points are allocated on the lower surface of the bow segment of the catamaran as a simulation of the Piezotronics transducers in experimental tests. The reason is to study the manner of pressure which is highly dependent on recorded position, that these variable factors are the impact angle, plate curvature, amount of water, and water velocity. Thus for an accurate comparison, the exact locations are taken from the experimental tests, in Swidan et al. (2017), which are summarized in Table 6. For the sake of brevity only the diagram for $V_{impact} = 5$ m/s represented, in a comparative shape for each transducer separately, Fig. 8 the results indicate that acceptable values for error percentage.

The main criteria are the maximum pressure of different transducers which are located at the archways beneath the wet deck, p-1 is located farthest from the outer part and p-5 is the outermost transducer. The exact deviation for each transducer is different, E = −15.4%, +10%, +6.5%, +8.3%, +5% are the error values for p-1 to p-5 respectively, Fig. 13. The question is why there were different error percentages for each transducer. The main reason is the different impact conditions involved in velocity and angle of impact. As previously said in the 2D wedge water entry validation, the accuracy of all numerical solutions varied in different conditions, for instance, in the present study which is validated with other methods the deviation could vary between e = 5% to e = 29% for a wedge with a deadrise angle of $\beta = 35°$, and $\beta = 15°$ respectively. as the impact angle is bigger, the related error percentage larger due to complex phenomena such as air compressibility or air entrapment, and air cushioning effects.

To better conceptualize the water entry issue, a series of VOF snapshots of velocity contour is implemented, basically based on the volume fraction of air, water, and free surface, Fig. 14. The velocity range is, $0 < u < 15$ m/s, for all time steps, the initial impact velocity is $V_{impact} = 5$ m/s. logically, as time goes on the velocity of water particles experienced a larger magnitude velocity especially for the zones between two demi-hull due to water entrapment. In other words, the accelerated water particle blocked with the bow hull generates a layer of compressed air which creates a shock pressure, that these high air pressures vented and run away through archways to some extent. The present paper aims to facilitate the existence of high-pressure air by implementing extra physical instruments within the bow structure, and ventilation pipes which are completely discussed in the next sections.
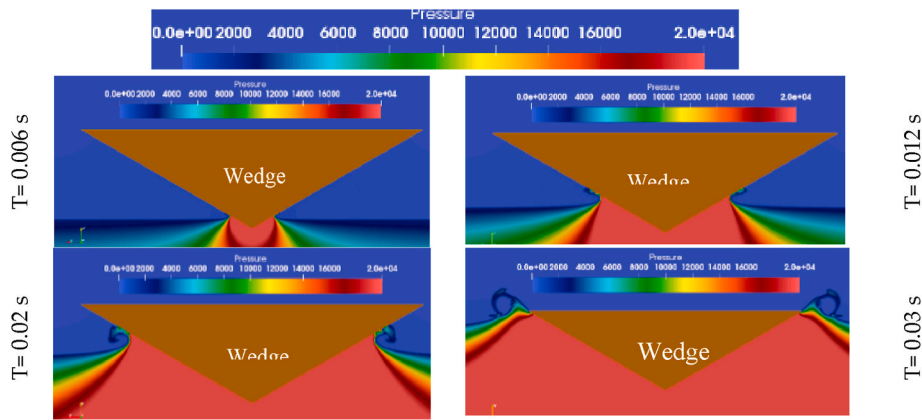
Table 4
The wedge impact condition for different test numbers.

Test. NUM	I	II	III	IIII	V
Deadrise Angle	15°	20°	25°	30°	35°
Falling height	0.5m	0.5m	0.5m	0.5m	0.5m

Fig. 11. The representation of the pressure contour of the wedge impact ($\beta = 30°$), in different penetration depth.
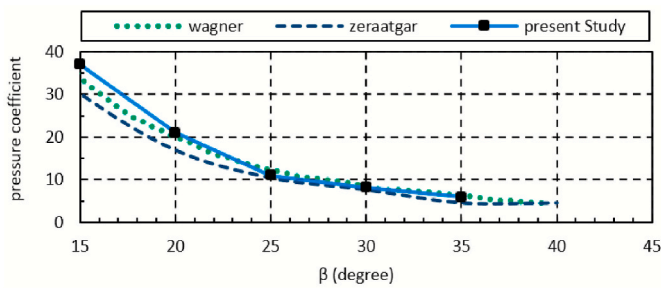

Fig. 12. Comparison of pressure coefficient versus wedge deadrise angle by considering three different methods.

Table 5
The overall characteristics of the scaled INCAT catamaran.

Dimension	Value	Unit	Schematic view
Overall bow section Length	0.5	m	
Beam	0.628	m	
Height	0.327	m	
Depth to the wet deck	0.145	m	
Depth to the center bow	0.06	m	

Table 6
The exact location of the five hypothesis transducers.

Transducer/Location	x (mm)	y (mm)	z (mm)
P1	111.06	96.82	165.62
P2	105.98	135.53	173.08
P3	100.9	174.25	180.53
P4	95.82	212.95	187.99
P5	90.74	251.67	195.45

3. Results and discussion

3.1. Scope of the study

The ship-slamming phenomenon departs into bottom impact, bow-flare impact, and wet deck slamming, depending on water entry angle and velocity, penetration depth, wave position, and hull form (Bertram, 2000). Generally, a catamaran's bottom profile is involved two high steepness slender bodies with a small waterplane area compared to some monohulls with a flat and huge bottom shape. This caused the lower magnitude of slamming force imposed on the bottom profile. However, in the case of wet deck slamming, the imposed forces could be very destructive for the catamarans' structure due to the large deck area; this structural weakness will be significantly improved by adding a center bow beneath the main deck (Thomas et al., 2003). The recent studies on the air cushioning effect are: Mai et al. (2019) experimentally investigated a rigid plate free-falling for two cases, aerated and non-aerated conditions, and they concluded that the aeration could decrease the impact load. Truong et al. (2021) used the fluid-structure interaction method to assess the air cushioning effects on a flat-stiffened plate, especially for a small deadrise angle. Zhang et al. (2018) numerically investigated how the slamming force changes air compressibility by using the different aspect ratios of perforated plates.

As Zhu and Faulkners' findings (Zhu et al., 1995) show, for a wet deck slamming of a Small Water-plane Area Twin-Hull (SWATH), the deadrise angle is critical for the maximum pressure and slamming force. Such that, among the considered cases (deadrise angle between $\beta = 0°$ and $\beta = 20°$) the case with $\beta = 4°$ Deadrise angle had the maximum value, but the question is, why? They inferred that the air entrapment for this deadrise angle induced extra pressure into the structure. Thus, further investigation needs to understand to what extent the cumulative pressure could change the slamming load imposed on the structure.

There were many databases and classified rules for conventional marine vessels in classification societies and companies. However, for a novel craft like catamarans, especially the big ones, the innovative idea will need further investigation to have comprehensive comparative results, particularly for severe conditions, like, wet decks and slamming events. INCAT is a catamaran with a center bow and surface-piercing demi-hull built by INCAT Tasmania. This company is in Australia, a leading company in building Wave-Piercing Catamaran (WPC) exceptionally large with high operational speed. As expected, the demi-hulls generate low reserve buoyancy; therefore, an additional structure, the "center bow," is used to decrease the vessels' downward moves, especially for pitch rotation. This extra buoyancy reduces the impact velocity and loads imposed on the structure.

3.2. Adding ventilation pipes

In the present study, a scaled model of a 112 m INCAT catamaran is used by considering only the vessels' bow segment to investigate the slamming phenomenon within the added ventilation pipes through the bow structure. The air bubbles and water syntax generate an air cushion beneath the vessel's structure (Faltinsen, 1993). Matveev, 2020 (Matveev, 2020) numerically investigated the injected air to the underwater
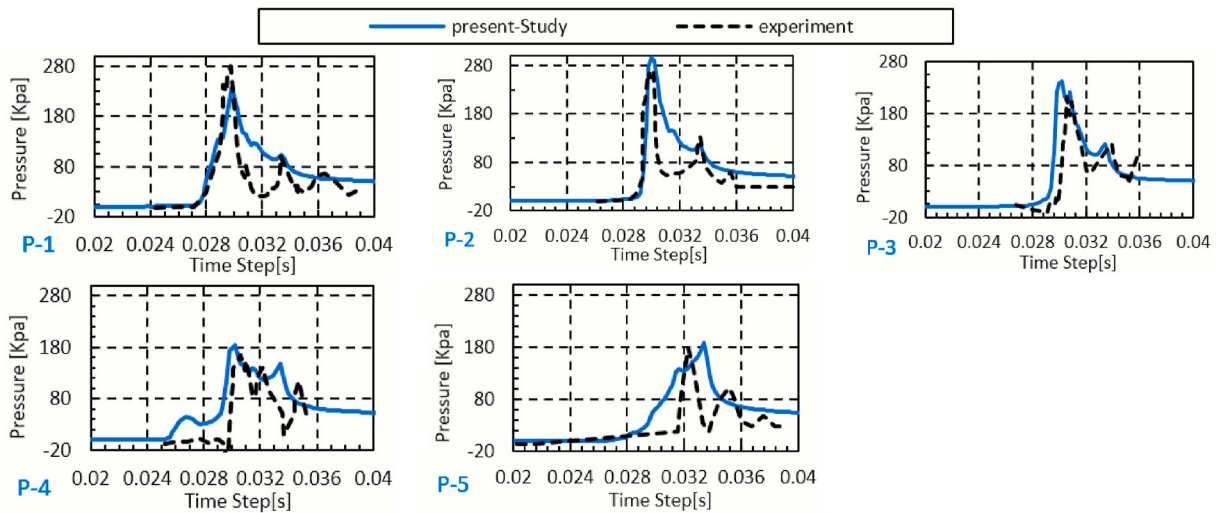
Fig. 13. A complete comparison of five distinct transducers for the present numerical solution against experimental results with $V_{impact} = 5 \, m/s$

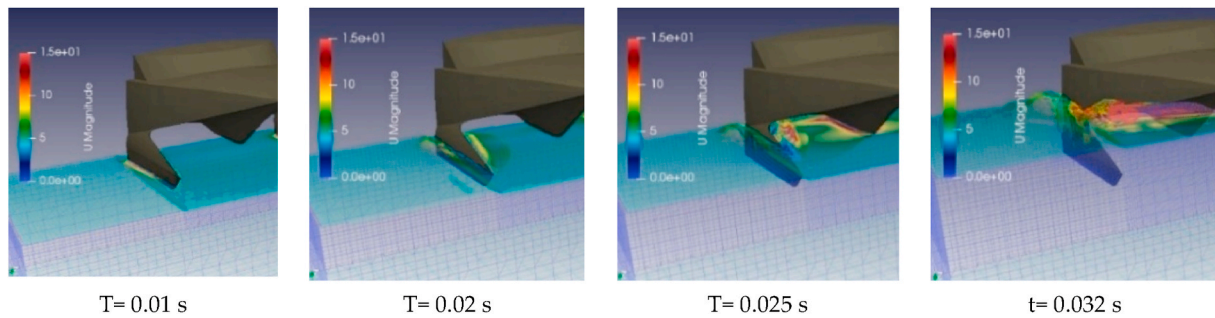| T= 0.01 s | T= 0.02 s | T= 0.025 s | t= 0.032 s |

Fig. 14. The VOF view of the 3D bow section impact of INCAT catamaran involved velocity contour for free surface velocity.

surface of marine vessels that caused Air-Cavity flow. The entrapped air has positive and negative effects: positive; air cushion could change the pitch and heave added mass coefficient (Chenu et al., 2004), causing less immersion into the water, which prevents high penetration depth for the bow section. Accordingly, Swidan (2016) used a winged-shaped center bow to increase the air cushion due to generated flow separation during the impact. The variation in the added mass coefficient also decreases the mean slamming force peak by about 6% rather than the case without the winged center bow. Negative; the air bubbles are trapped such that: whatever the bow penetrates the water, the air becomes condensate; this compressed air imposes a large amount of pressure and force on the structure, which causes stress on the unprotected wet deck structure.

A feasible and straightforward solution to decrease the cumulative pressures beneath the deck, especially at the archways, is "Air ventilation pipes," performed with three pipes located at the top of the archways, Fig. 15. The extra transferred pressure into the atmosphere causes pressure reduction, particularly when the water rises the sidewall of the demi-hulls and reaches near the archways. There are two aspects of ventilation pipes installation; first, how to install it "some stiffeners or any stiffened panels may need around the pipes, even a little change in bow structure." Second, the variations in structural strength besides the stress and strain behavior in critical conditions. Although there is no need for any fundamental changes in the structural platform, further structural analysis needs to predict the hull strength correctly. The present study is only focused on the hydrodynamic effect, which is more important to assess the applicability of the proposed idea; structural behavior could be studied in future research.

The selection criteria for the location, numbers, and diameters of ventilation pipes are considered the most viable solution to increase the amount of ventilation air beside the least structural strength.

- Three inputs provide to cover the entire space above the arch closure. This could support three separate pipes or a single three-way pipe: in this research, a three pipes system is considered for simulations.
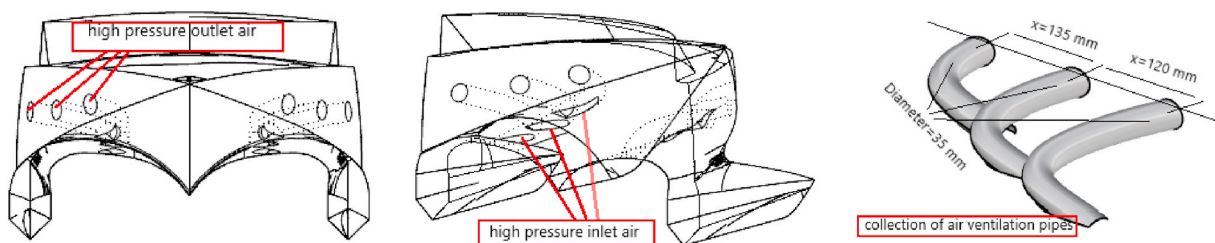

Fig. 15. Schematic of bow section for a standard INCAT wave-piercing catamaran with air ventilation pipes (amended catamaran).

- The diameter is not very big, which is not needed for an air ventilation system, and is not too small, which lowers the amount of ventilation air.
- The pipe's entrance positions are in the middle and the top line of the arc closure, which is the end of immersion.

3.2.1. Define different impact conditions

The 2D and 3D numerical solutions could be an efficient way to recognize the pressure values in slamming. However, 2D cases are very cost-efficient and could be a good choice for issues without a closure, like simple wedge and monohull vessels. The structures with a closure like catamarans influence by severe air and water entrapment; it is not accurate enough to use 2D simulations. For the present case, to better capture the air entrapment effects and further use the number of air ventilation pipes, using 3D simulation is reasonable. Another important issue is that the lateral loads imposed additional stress on the catamaran's structure than on the monohull; complete simulation is performed for three main impact conditions, including 12 case studies, Table 7; the impact velocities are V = 2 to 5 (m/s) in $\Delta V = 1$ (m/s) increment.

During the slamming, the amount of air venting from archways, the amount of air and water mixture, and the cumulative pressure beneath the wet deck caused different manners with different velocities and impact angles. The air pressure discrepancies affect two critical factors, the air cushion and the load imposed on the structure, especially the top of the demi-hull truncation. Although air cushion caused extra load into the structure, the changes in added mass coefficient could decrease the slamming penetration depth and velocity. This process involved air transfer, air cushion, and the variations of air pressure called the aeration phenomenon that should consider in the designing process, especially for center bow catamarans.

3.2.2. Pressure distribution results

The ventilation pipes are high-pressure discharger tools for severe slamming conditions. The pipes inlet could have an adjustable entrance depending on the incident pressure values; for instance, when the pressure gets to the designated value, the gate opens, and the pressure discharges into the air. Pressure evaluation involves three main factors: maximum pressure, pressure propagation, and pressure distribution, all of which mention in the present study. For the amended catamaran, two arrays of pressure gauges are set on the body's surface beneath the wet deck to have more precise results. The positions and the exact locations are mentioned in Table 8; these pressure gauges are created by ParaView, a postprocessing tool for OpenFOAM.

The analyzed pressures mechanism captures the maximum absolute pressure and distribution. All the engaged sensors show a reduction in pressure values. Fig. 16 illustrates the pressures on the parent and amended hull of case II (pitch = 5°) and case I (no-motion), impact velocity, V = 2 m/s, and V = 4 m/s respectively. The magnitude pressure value and time of occurrence changed noticeably by adding the air ventilation pipes, whereas the maximum recorded pressure decreased by about 31.7% and 40%, respectively. The occurrence time changed from t = 0.071 s to t = 0.073 s for case II and from t = 0.037 s to t = 0.038 s for case I. It is noteworthy that adding ventilation pipes decreases the cumulative pressure significantly.

These results are also valid for the maximum impact velocity (V = 5

m/s) with less intensity; the maximum pressure shows a 14.7% decrease in value and dt = 0.001s delay in occurrence time, Fig. 16. Surprisingly adding ventilation pipes caused the decreasing rate in some gauges by about 50% (G-4 and G-5 for V = 5 m/s). To evaluate the influence of the impact velocity for the parent and amended hull, the cross-section for the rear pipe of case II is considered, Fig. 18. As could be inferred, although the pressure field for the amended hull is lower than the parent hull for all impact velocities, the most significant difference in pressure value belongs to V = 2 m/s.

Why do the pressure discrepancies between the parent hull and the amended hull decrease for higher impact velocity (Fig. 17)? The answer is "chance of air escape," the ventilation pipes' efficiency is highly dependent on the rate of air outflow within a specific time; thus, to what extent the impact velocity is smaller (V = 2 m/s), the volume of the outflow air increase; as a result, the pressure goes down. In addition to the ventilation pipes that decrease the pressure largely beneath the wet deck, the impact duration has a notable effect on pressure distribution, which means the shorter the impact duration, the "higher impact velocity," the sooner water will hit the deck, and there will be less time to discharge the cumulative pressure and air escaping.

To better investigate the effects of ventilation pipes, the results of ten gauges (G-1 to G-10) consider for case III (Roll = 10° & Pitch = 5°), impact velocity, V = 2 m/s represented in Figs. 19 and 20. The maximum pressure reduction of about 40% for the gauges G-1 to G-5, the position of these gauges, at line y = - 0.1 m near the center bow, but for the gauges located at line y = − 0.2 m, G-5 to G-10, the reduction rate is not comparable with the former line, just about 10% decrease in maximum pressure.

For the left section of the hull, the points near the CBT (Center Bow Truncation) experienced more pressure apart from considering the ventilation pipes or not, $p_{max} = 67000$ [pa] for the parent hull and $p_{max} = 60000$ [pa] for the amended hull. The left side of the catamaran impacts water with more intensity than the right side, Fig. 21; this leads to moving the water particles to the sections near the CBT and front half of the catamaran with a higher pressure value, that the run-up water during impact imposed more pressures on the G-5 to G-10.

A large amount of water could escape in any direction for the pressure gauges near the unprotected deck (G-5 and G-10); thus, these gauges have lower pressure values than the gauges within the arch closures. The structural force decreases significantly when the water transfers into the open area. This effect could be different for each impact angle, whereas the discrepancy is significant for the standard model with zero pitch angle, and as much as the pitch angle increase, the difference becomes less. Another conclusion behind the assessments is the pressure variations due to the geometry and impact condition, causing more or less water to escape beneath the deck. Although ten pressure gauges use to show these variations, slamming coefficients are still not widely explored for varying body geometrical shapes. Indeed, the geometrical shape will affect air entrapment capabilities that directly impact the slamming pressure or slamming coefficient in design guidelines. Future work could connect the relationship between the waterplane area coefficient and the slamming coefficient.

Further, the impact angle and the impact velocity could also affect the pressure distribution. The faster the impact, the lower the discrepancy, lowering the chance of water escape. For better orientation in the velocity discrepancies, Fig. 22 compares the influence of adding ventilation pipes for case III (Pitch = 5° & Roll = 10°) at V = 2, 3, 4, 5 m/s, the cross-section contours allocated at the rear pipe, and the velocity field is represented for the whole domain, that the maximum particles' velocity appeared beneath the wet deck near the center bow.

3.2.3. Velocity and pressure stream-lines distribution

The innovation of the present study is using ventilation holes beneath the wet deck, such that the extra pressure could transfer to the atmosphere through these pipes. To illustrate the pipes' operation better, the streamlines for the two main variables, pressure, and velocity,

Table 7
The main case studies' impact situation parameter.

| case	Roll	Pitch	Yaw	Impact velocity (m/s)
I	$\theta = 0$	$\omega = 0$	$\alpha = 0$	V = 2, 3, 4, 5
II	$\theta = 0$	$\omega = 5°$	$\alpha = 0$	V = 2, 3, 4, 5
III	$\theta = 10°$	$\omega = 5°$	$\alpha = 0$	V = 2, 3, 4, 5

Table 8
Pressure gauges position in the principal coordinates fx3.fx4.

Gauge number	G-1	G-2	G-3	G-4	G-5	G-6	G-7	G-8	G-9	G-10
X (meter)	0.05	0.1	0.15	0.2	0.25	0.05	0.1	0.15	0.2	0.25
y (meter)	0.1	0.1	0.1	0.1	0.1	0.2	0.2	0.2	0.2	0.2
	Parent hull					Amended hull				
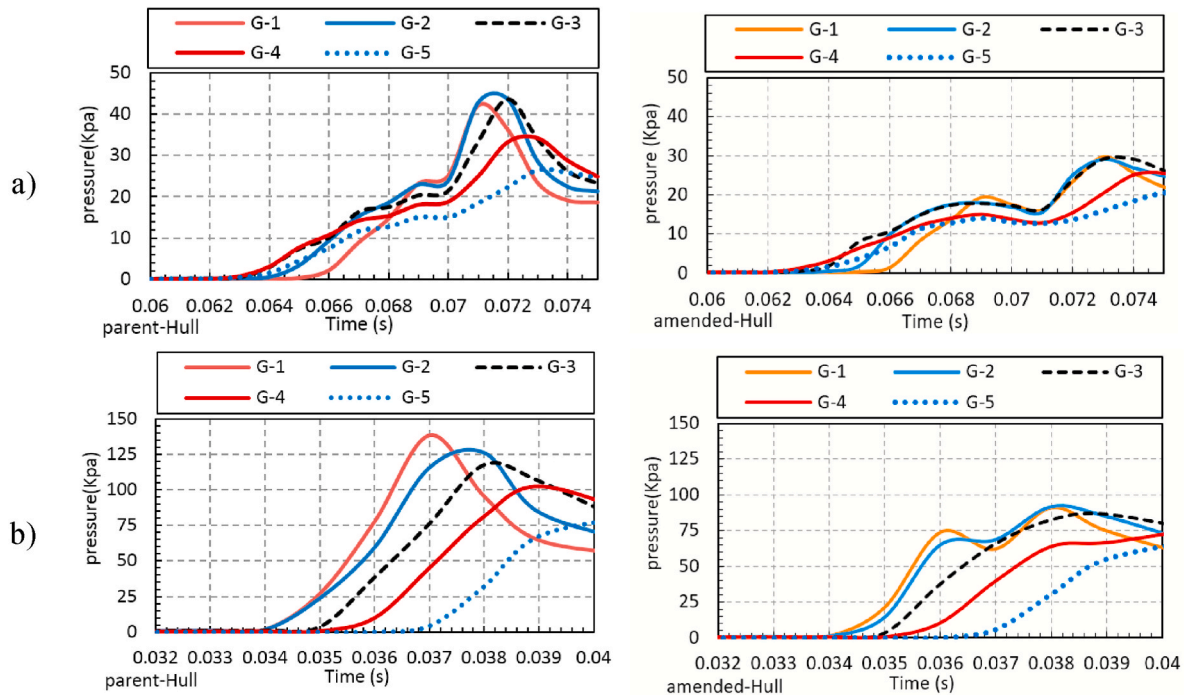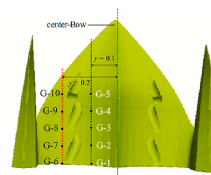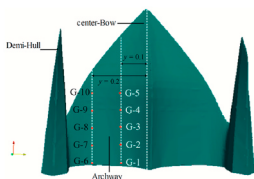
Fig. 16. Pressure gauge (G-1 to G-5) values, parent and amended hull, a) case II (V = 2 m/s), b) case I (V = 4 m/s).
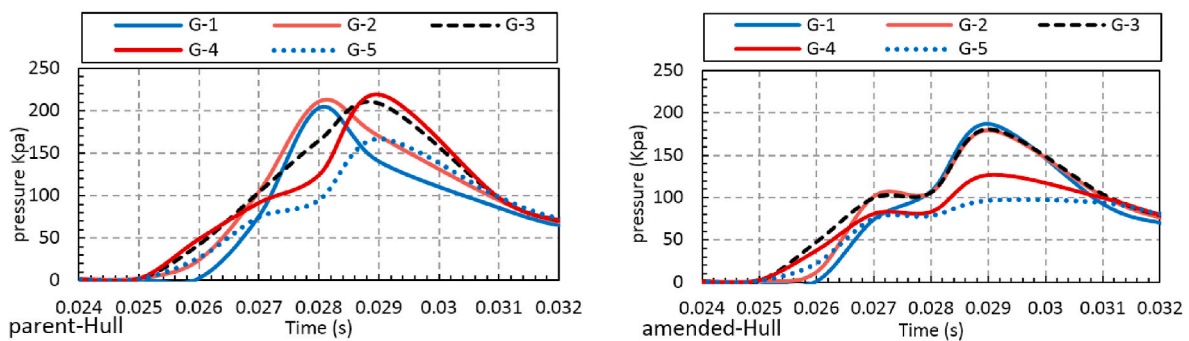
Fig. 17. Pressure gauge (G-1 to G-5) values for parent and amended hull, case II with V = 5 m/s.

are shown in Figs. 23 and 24, respectively. They are gathered for four time-steps, t = 0.023, 0.026, 0.029, 0.032 s, case (I) with V = 5 m/s. The rate and the value for each pipe could be different depending on the position of entrance holes, the impact angle and velocity, and the pipes' dimensions.

For the present study, the diameter of the three pipes is similar, D = 100 mm, and the only difference is the position and size of the inlet holes. The pipe's position divides into three categories, rear pipe, middle pipe, and front pipe. The air is entrapped in the middle; thus, the middle pipe is more important than other pipes where the pressure escapes from the open areas; this leads to a higher value for transferred fluid within the middle pipe than in others, Fig. 24.

Further to the pressure, the fluid particle velocity involving air and water is an influential parameter; accordingly, further streamlines are
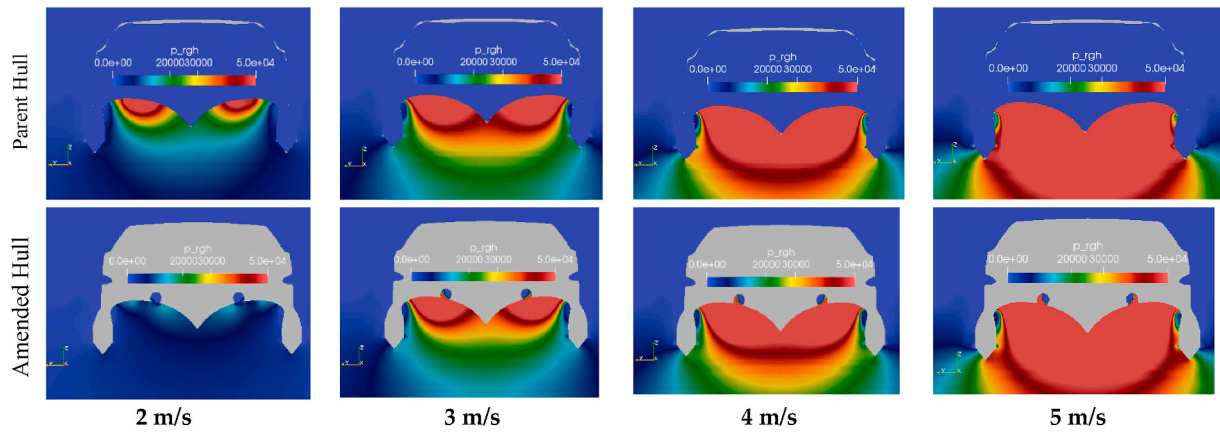
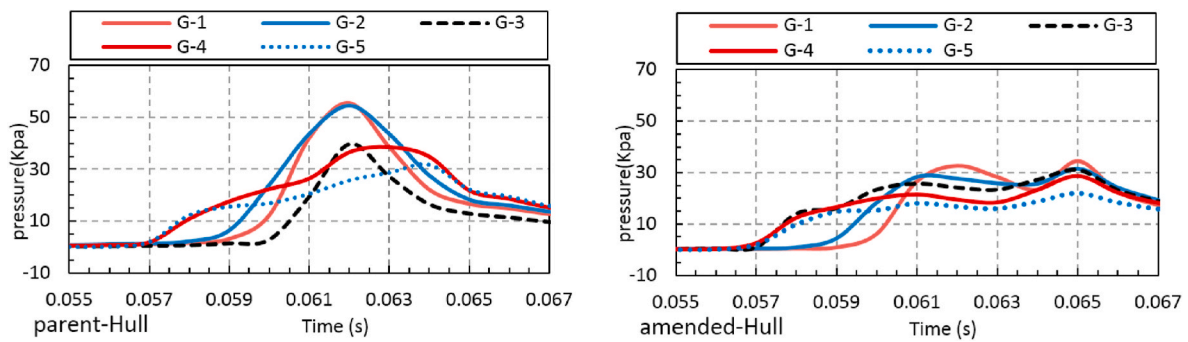**Fig. 18.** The maximum pressure contour for the parent and amended hull at a different impact velocity.

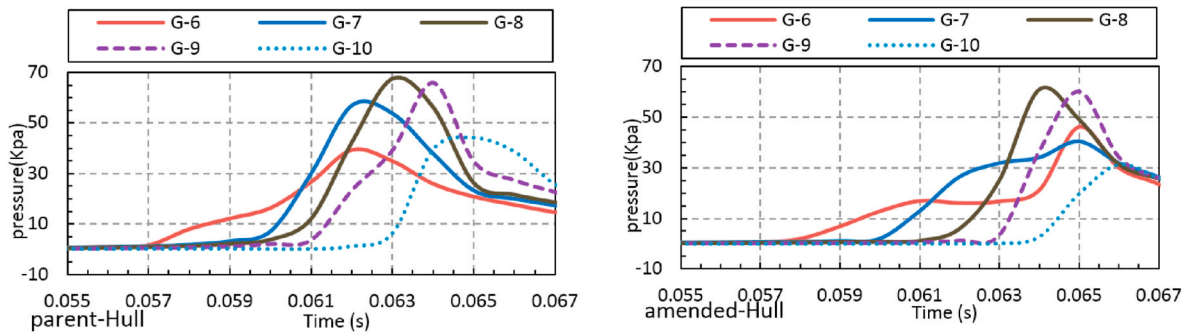**Fig. 19.** Pressure gauge (G-1 to G-5) values for parent and amended hull, case III with V = 2 m/s.

Fig. 20. Pressure gauge (G-6 to G-10) values for parent and amended hull, case III with V = 2 m/s.

used based on the velocity for case I (V = 5 m/s), Fig. 23. As illustrated, the range of velocity contour is $0 < u_{magnitude} < 30(m/s)$, same as the pressure streamlines, the middle pipe's particle velocity is higher than others, especially for t = 0.023 s and t = 0.026 s. Although the entrance position and size mainly influence the transferred rate of energy, the shape and size of the pipes involved, pipes' diameter, pipes' length, inlet & outlet shape, and dimensions could also change the energy flux.

3.2.3.1. Slam force assessment for amended catamaran. Aluminum alloys and composite materials are widely used in catamaran structures to reduce the vessel's weight and increase the cruise speed, besides efficient fuel consumption. Thus the vessel's hydrodynamic loads at different sea states are the most significant issue in the designing process; this analysis is more critical for the big catamaran with more cruise speed and complex bodies' form (Heggelund et al., 2002), (Roberts et al., 1997). The catamarans bore a large amount of force during the

slamming, especially catamarans with a center bow. The slam event occurred in a bit of time, and an enormous pressure and force acted on the structure; these pressures trapped between the demi-hulls, center bow, and the free surface. In the last section, a complete investigation is performed on the pressure variations and values; thus, in this section, a force analysis needs to perform individually.

The structural force could be evaluated by implementing two methods in OpenFOAM, first using force libraries "functionObjectLibs" as an external code added to the standard model by substituting in controlDict. These functions are solved together with the main solver at each time step. The second method uses a postprocessing tool for OpenFOAM solvers, ParaView; this software could simultaneously use as the graphical and computational tools. In the present study, ParaView is used to calculate the imposed forces on the structure, which involve some main steps: extract the surfaces, calculate the normal vector on the surface, multiply the calculated pressure by the normal vector, and finally integrate the forces for all the structure, the simple dominant
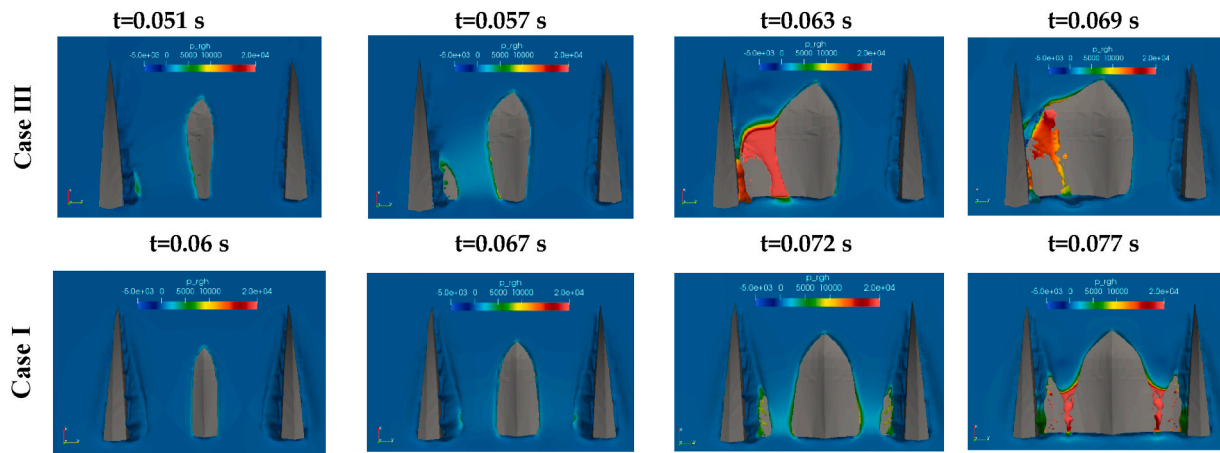
Fig. 21. The pressure distribution on the free surface during the impact for the case I and case III at different time steps.
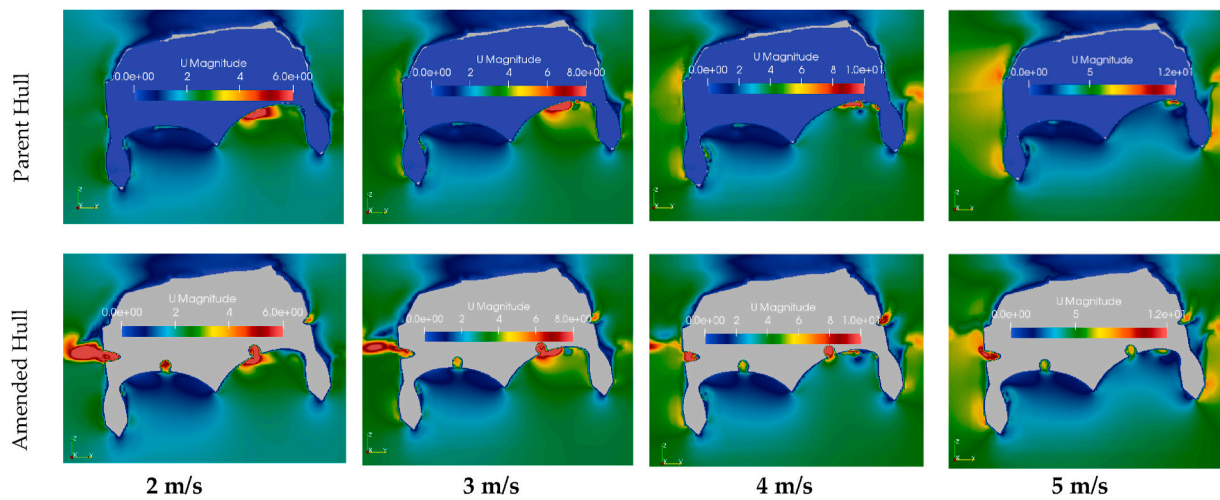

Fig. 22. A contour-based comparison for the amended and parent hull of the magnitude velocity for different impact velocities, V = 2, 3, 4, 5 m/s.
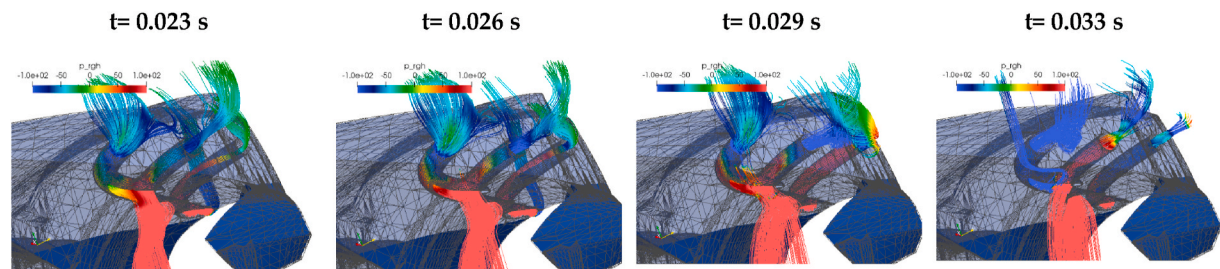

Fig. 23. The streamlines contour of the magnitude pressure, t = 0.029, 0.026, 0.029, 0.033 S.

formula is:

$$\overrightarrow{F} = \sum s_i \overrightarrow{n_i} p_i \qquad (22)$$

where F is the total force, S_i is the area of the face (i), n_i is the normal vector of a face (i), and P_i is the pressure on the face (i). The accuracy of the pressure was verified in the last section; thus, there is no need for further validation; indeed, the calculated forces based on formerly verified pressures are accurate enough. As expected, due to pressure decrement for the amended hull observed in the previous sections, the results for three different positions at the slamming tests of the INCAT catamaran case (I, II, III) also show a reduction of slamming force.

The maximum slamming force for the parent hull is F = 18, 27, 22

[KN], and for the amended hull is F = 15.7, 21.5, 19.2 [KN] with a reduced rate of 13%, 18%, 13% for case (I, II, III), respectively, Fig. 25, this trend is true for other impact velocities. Another phenomenon to mention is the slamming force for case (III), which has two peaks, that is because the Roll angle (θ = 10°) whereas, in impact threshold, only the left section of the body enters to water which causes lower force, and as time goes on, the right section of the hull also impacts water, causing a second force peak in diagrams, Fig. 26.

In all case studies, the slamming force is plotted versus the impact velocity for the parent and amended hull, Fig. 27. The pace of change is similar for both the amended and parent hull, but the values are different. Furthermore, the Pitch motion (Pitch = 5°) increase the force
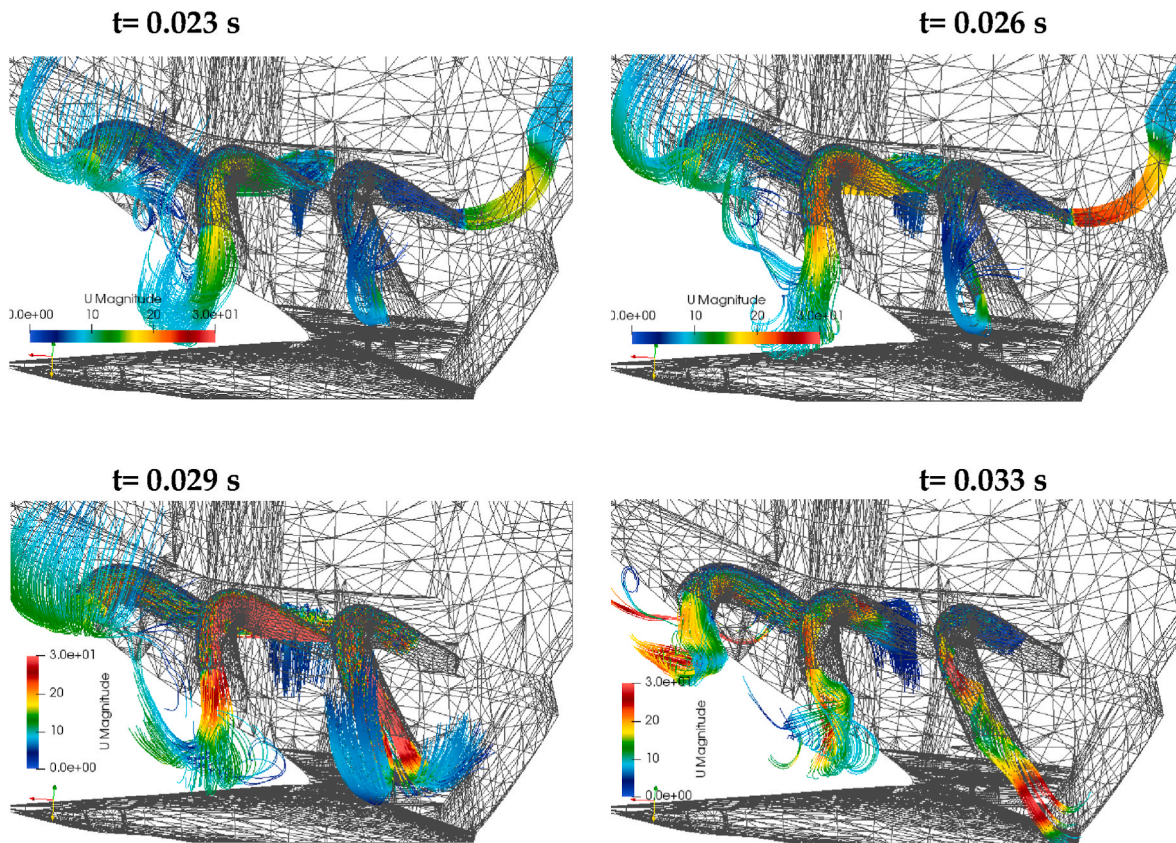
t= 0.023 s　　　　　　　　　　　　**t= 0.026 s**

t= 0.029 s　　　　　　　　　　　　**t= 0.033 s**

Fig. 24. The streamlines contour of the magnitude velocity for, t = 0.029, 0.026, 0.029, 0.033 S.

Roll = 0 & Pitch = 0 (case I)　　　Roll = 0 & Pitch = 5° (case II)　　　Roll = 10° & Pitch = 5° (case III)
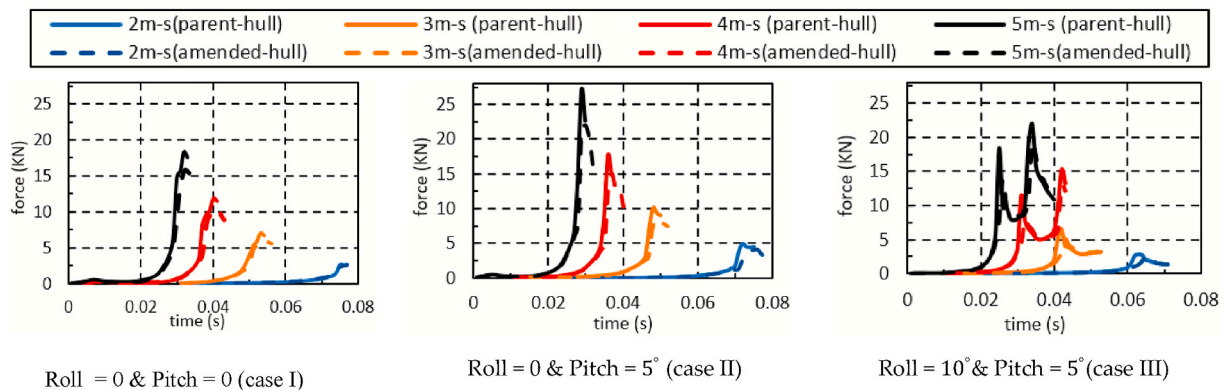
Fig. 25. Slamming force comparison for three cases, cases I (a), II (b), and III (c), for different impact velocities.

imposed on the structure significantly, but the Roll motion (Roll = 10°) reduce this incremental value for V = 2 m/s and V = 3 m/s. The reduction is such that the force becomes lower than the vessel without any motion. In fact, the Roll motion could decrease the slamming force, unlike the Pitch motion.

The question is, why do these force variations occur for Pitch and Roll angles? The reason is "the angle of impact," The smaller the angle of impact, the more forces and pressure are applied to the structure. Pitch motion decreases the longitudinal angle relative to the free surface, increasing the pressure on the vessel's hull. For case III, besides the Pitch angle, a Roll angle adds to the impact condition; thus, the left angle decreases, but the right angle increases; this condition is asymmetric impact, completely explained in Masoomi et al. (2017). For the left side, a significant portion of the pressure is imposed on the side body and others are applied beneath the deck; besides, the right of the hull

experience lower pressure due to the big impact angle, causing a smaller force summation in comparison with standard impact condition.

4. Conclusion

Two major steps need to introduce the idea behind the slamming phenomenon's aeration process: first, determining the optimal numerical solution for the water entry of a big and complicated body, and second, designing and installing the system on the scaled model of 112 m Incat Tasmania catamaran to test the model applicability. In the first step, the static (fixed-body and static mesh) or dynamic (moving-body by considering the OverSetMesh technique) is solved by considering the RANS equation with standard OpenFOAM libraries. The final results compared with experiments, the fixed-wedge had an accurate result besides low computational cost; thus, selected as the primary approach
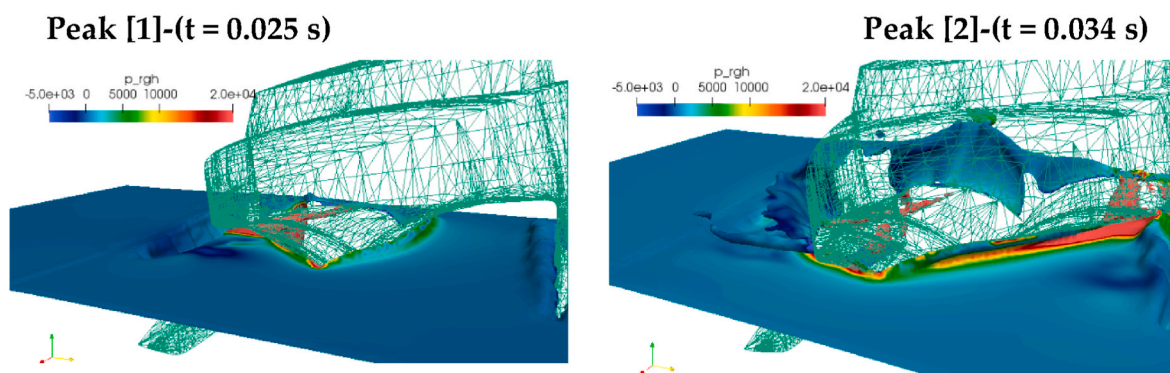
Peak [1]-(t = 0.025 s)

Peak [2]-(t = 0.034 s)

Fig. 26. Pressure contour for case III with V = 5 m/s for two pressure peaks.
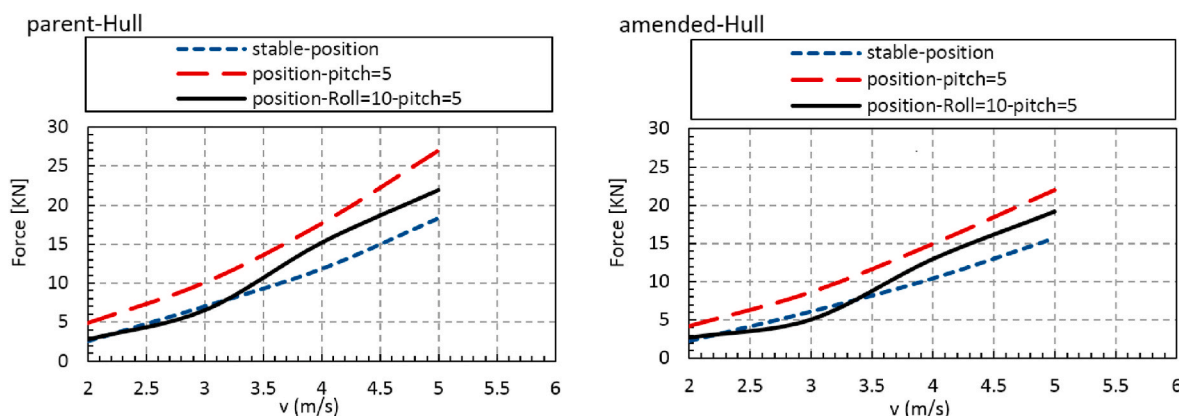

Fig. 27. Slamming force comparison for the amended and parent hull versus different impact velocities.

for simulating the catamarans' slamming behavior. This paper represents an innovative strategy to reduce the pressure and slamming force imposed on the bow section of the wave-piercing catamaran, which has not been tested before; thus, different case studies apply to have comprehensive results (12 case studies). A brief description of the idea is adding three similar ventilation pipes within the deck structure; the inlets located beneath the wet deck and outlets are such to discharge the extra pressure into the atmosphere. From the structural aspect, the advantage and limitations of this ventilation system are:

Advantages.

- Discharging the high-pressure air into the atmosphere reduces momentary severe slamming force.
- No external system adds to the parent hull, which does not affect the vessel's hydrodynamic.
- This system adds on the formerly built catamarans with some extra modifications.
- This system's inlet or outlet gates could be controllable depending on different operational conditions.

Limitations.

- The layout must be such that the bow structure does not transform into a vulnerable structure.
- The input ducts must be positioned at the top of the arch closure to have utmost efficiency and prevent the water currents from entering the pipes.

The results indicate that the ventilation pipes significantly decrease the pressure and slamming force apart from the impact condition, and the reduction rate depends on the impact condition. The recorded

pressure positively correlates with the impact condition and the ventilation pipes' position; thus, ten pressure gauges define virtually. The interval of changes for the pressure was between 15% and 50%, and the maximum recorded slamming force was when the free surface reached the top of the archways and raised the cumulative pressure to the maximum value. Same as the pressure recorded values, the results for slamming forces were also different depending on the impact conditions; the rate of change was approximately 5%–25%.

The fundamental question is, how added ventilation pipes reduce the pressure and slamming loads? The answer is ventilated air through these pipes; as illustrated by contours in this paper, a large amount of trapped pressure discharges into the atmosphere, depending on the impact condition and pipes' dimensions and layout. In conclusion, although air ventilation pipes decrease the air cushion volume and change the added mass coefficients, which causes more immersion in water, these pipes decrease the load imposed on the structure. The represented system has two sides; one is positive, "decreasing the pressure and imposed force on the catamaran's structure." The other is negative "losing part of the air cushion effect and more immersion to water," the resultant reduction rate of pressure and slamming force compensates for the increment due to losing the air cushion effect.

Declaration of competing interest

The authors declare that they have no known competing financial interests or personal relationships that could have appeared to influence the work reported in this paper.

References

Aagaard, O., 2013. Hydroelastic Analysis of Flexible Wedges. Institutt for marin teknikk.
Afshar, M.A., 2010. Numerical Wave Generation in OpenFOAM®.

Almallah, I., et al., 2021. Slam load estimation for high-speed catamarans in irregular head seas by full-scale computational fluid dynamics. Ocean Eng. 234, 109160.

Barjasteh, M., Zeraatgar, H., Javaherian, M.J., 2016. An experimental study on water entry of asymmetric wedges. Appl. Ocean Res. 58, 292–304.

Batina, J.T., 1991. Unsteady Euler algorithm with unstructured dynamic mesh for complex-aircraft aerodynamic analysis. AIAA J. 29 (3), 327–333.

Berberović, E., et al., 2009. Drop impact onto a liquid layer of finite thickness: dynamics of the cavity evolution. Phys. Rev. 79 (3), 036306.

Bertram, V., 2000. Resistance and Propulsion. Practical Ship Hydrodynamics. Butterworth-Heinemann, pp. 62–95.

Borg, S.F., 1957. Some contributions to the wedge-water entry problem. J. Eng. Mech. Div. 83 (2), 1214, 1-1214-28.

Campana, E., et al., 2000. Parametric analysis of slamming forces: compressible and incompressible phases. J. Ship Ocean Technol. 4 (1), 21–27.

Cheng, H., et al., 2020. Ship hull slamming analysis with smoothed particle hydrodynamics method. Appl. Ocean Res. 101, 102268.

Chenu, B., Morris-Thomas, M., Thiagarajan, K., 2004. Some hydrodynamic characteristics of an air-cushion supported concrete gravity structure. In: Proceedings of the 15th Australasian Fluid Mechanics Conference. Citeseer, Sydney, Australia.

Cointe, R., Armand, J.-L., 1987. Hydrodynamic Impact Analysis of a Cylinder.

Damián, S.M., Giménez, J.M., Nigro, N.M., 2012. gdbOF: a debugging tool for OpenFOAM®. Adv. Eng. Software 47 (1), 17–23.

Davis, M.R., Whelan, J.R., 2007. Computation of wet deck bow slam loads for catamaran arched cross sections. Ocean Eng. 34 (17–18), 2265–2276.

Doustdar, M.M., Kazemi, H., 2019. Effects of fixed and dynamic mesh methods on simulation of stepped planing craft. J. Ocean Eng. Sci. 4 (1), 33–48.

Fairlie-Clarke, A., Tveitnes, T., 2008. Momentum and gravity effects during the constant velocity water entry of wedge-shaped sections. Ocean Eng. 35 (7), 706–716.

Faltinsen, O., 1993. Sea Loads on Ships and Offshore Structures, vol. 1. Cambridge university press.

Faltinsen, O., Chezhian, M., 2005. A generalized Wagner method for three-dimensional slamming. J. Ship Res. 49 (4), 279–287.

Ferziger, J.H., Perić, M., Street, R.L., 2002. Computational Methods for Fluid Dynamics, vol. 3. Springer.

Fraenkel, L., McLeod, J., 1997. Some results for the entry of a blunt wedge into water. Philos. Trans. R. Soc. London, Ser. A: Math. Phys. Eng. Sci. 355 (1724), 523–535.

French, B.J., Thomas, G.A., Davis, M.R., 2015. Slam occurrences and loads of a high-speed wave piercer catamaran in irregular seas. Proc. IME M J. Eng. Marit. Environ. 229 (1), 45–57.

Garabedian, P., 1953. Oblique water entry of a wedge. Commun. Pure Appl. Math. 6 (2), 157–165.

Gopalan, H., Jaiman, R., Chandar, D.D., 2015. In: Flow Past Tandem Circular Cylinders at High Reynolds Numbers Using Overset Grids in OpenFOAM. *53rd* AIAA Aerospace Sciences Meeting.

Greenhow, M., 1987. Wedge entry into initially calm water. Appl. Ocean Res. 9 (4), 214–223.

He, W., et al., 2013. URANS study of Delft catamaran total/added resistance, motions and slamming loads in head sea including irregular wave and uncertainty quantification for variable regular wave and geometry. Ocean Eng. 74, 189–217.

Heggelund, S., Moan, T., Oma, S., 2002. Determination of global design loads for large high-speed catamarans. Proc. IME M J. Eng. Marit. Environ. 216 (1), 79–94.

Hidalgo, V., et al., 2021. Rotatory 3D structured mesh study using openFOAM to simulate the flow in francis turbine. "Materials Today: Proceedings", 2021, vol. 49, núm. 1, p. 142-148.

Hirsch, C., Numerical Computation of Internal and External Flows, Vol. vol. 1, 2 *John Wiley k*. 1991, Sons, New York, NY.

Hirt, C.W., Nichols, B.D., 1981. Volume of fluid (VOF) method for the dynamics of free boundaries. J. Comput. Phys. 39 (1), 201–225.

Holzmann, T., 2016. Mathematics, Numerics, Derivations and OpenFOAM®. Holzmann CFD, Loeben, Germany.

Howison, S., Ockendon, J., Wilson, S., 1991. Incompressible water-entry problems at small deadrise angles. J. Fluid Mech. 222, 215–230.

Johannessen, S.R., 2012. Use of CFD to Study Hydrodynamic Loads on Free-Fall Lifeboats in the Impact Phase.: A Verification and Validation Study. Institutt for marin teknikk.

Kapsenberg, G., 1947. Slamming of ships: where are we now? Philosophical Transactions of the Royal Society A: Mathematical, Physical and Engineering Sciences, 2011 369, 2892–2919.

Korobkin, A., 1996. Water impact problems in ship hydrodynamics. Adv. Fluid Mech. 323–371.

Lavroff, J., et al., 2011. Determination of wave slamming loads on high-speed catamarans by hydroelastic segmented model experiments. Int. J. Marit. Eng. 153 (A3), 185–197.

Lee, S.B., 2017. A study on temporal accuracy of OpenFOAM. Int. J. Nav. Archit. Ocean Eng. 9 (4), 429–438.

Lin, Y., Ma, N., Gu, X., 2021. Potential-flow and CFD investigations of bow-flare slamming on a container ship in regular heading waves. Ocean Eng. 219, 108278.

Luo, H., Soares, C.G., 2012. Review of Model Test Techniques of Local Slamming on Ships. Maritime Engineering and Technology, Taylor and Francis, London, 189-194.

Mai, T., et al., 2019. Aeration effects on water-structure impacts: Part 1. drop plate impacts. Ocean Eng. 193, 106600.

Masoomi, M., Mosavi, A., 2021. The one-way FSI method based on RANS-FEM for the open water test of a marine propeller at the different loading conditions. J. Mar. Sci. Eng. 9 (4), 351.

Masoomi, M., Yousefifard, M., Ramiar, A., 2017. Numerical investigation of symmetry and asymmetry rigid wedge slamming using OpenFOAM code. Modar. Mechan. Eng. 17 (7), 343–352.

Matveev, K.I., 2020. Numerical simulation of air cavity under a simplified model-scale hull form. J. Ocean Eng. Sci. 5 (1), 68–72.

Mei, X., Liu, Y., Yue, D.K., 1999. On the water impact of general two-dimensional sections. Appl. Ocean Res. 21 (1), 1–15.

Mørch, H., et al., 2008. Simulation of lifeboat launching under storm conditions. In: 6th International Conference on CFD in Oil & Gas, Metallurgical and Process Industries. SINTEF/NTNU, Trondheim, Norway.

Muzaferija, S., 1999. In: A Two-Fluid Navier-Stokes Solver to Simulate Water Entry. Proceedings of 22nd symposium on naval architecture, 1999. National Academy Press.

Nair, V.V., Bhattacharyya, S., 2018a. Water entry and exit of axisymmetric bodies by CFD approach. J. Ocean Eng. Sci. 3 (2), 156–174.

Nair, V.V., Bhattacharyya, S., 2018b. Water impact of three dimensional wedges using CFD. Ocean Syst. Eng. 8 (2), 223–246.

Nikfarjam, M., et al., 2019. Evaluation of water impact for symmetric wedge by experimental and numerical methods. Int. J. Appl. Mech. Eng. 24 (1).

Nuernberg, M., Tao, L., 2018. Three dimensional tidal turbine array simulations using OpenFOAM with dynamic mesh. Ocean Eng. 147, 629–646.

O'Connor, C., Mohajernasab, S., Abdussamie, N., 2022. Numerical investigation into water entry problems of a flat plate with air pockets. J. Ocean Eng. Sci.

Oger, G., et al., 2006. Two-dimensional SPH simulations of wedge water entries. J. Comput. Phys. 213 (2), 803–822.

Oh, S., Kwon, S., Chung, J., 2009. A close look at air pocket evolution in flat impact. In: Proc. Of 24th International Workshop on Water Waves and Floating Bodies.

Panciroli, R., Shams, A., Porfiri, M., 2015. Experiments on the water entry of curved wedges: high speed imaging and particle image velocimetry. Ocean Eng. 94, 213–222.

Patankar, S., 2018. Numerical Heat Transfer and Fluid Flow. Taylor & Francis.

Roberts, T., Watson, N., Davis, M., 1997. Evaluation of sea loads in high speed catamarans. In: Fourth International Conference on Fast Sea Transportation.

Sasson, M., et al., 2016. A comparison between Smoothed-Particle Hydrodynamics and RANS Volume of Fluid method in modelling slamming. J. Ocean Eng. Sci. 1 (2), 119–128.

Shabani, B., et al., 2019. Slam loads and pressures acting on high-speed wave-piercing catamarans in regular waves. Mar. Struct. 66, 136–153.

Shah, S., Orifici, A., Watmuff, J., 2015. Water impact of rigid wedges in two-dimensional fluid flow. J. Appl. Fluid Mech. 8 (2).

Shahraki, J., et al., 2011. In: Prediction of Slamming Behaviour of Monohull and Multihull Forms Using Smoothed Particle Hydrodynamics. Proceedings of the 9th Symposium on High Speed Marine Vehicles (HSMV'11).

Sun, Z., et al., 2020. Investigation of trimaran slamming under different conditions. Appl. Ocean Res. 104, 102316.

Swidan, A.A.W., 2016. Catamaran Wetdeck Slamming: a Numerical and Experimental Investigation. University of Tasmania.

Swidan, A., et al., 2016. Experimental drop test investigation into wetdeck slamming loads on a generic catamaran hullform. Ocean Eng. 117, 143–153.

Swidan, A., et al., 2017. Wetdeck slamming loads on a developed catamaran hullform–experimental investigation. Ships Offshore Struct. 12 (5), 653–661.

Tang, H., et al., 2020. Numerical study of trimaran motion and wave load prediction based on time-domain Rankine-Green matching method. Ocean Eng. 214, 107605.

Thomas, G.A., et al., 2003. Transient dynamic slam response of large high speed catamarans. In: The 7th International Conference on Fast Sea Transportation. Ischia, Italy.

Thomas, G., et al., 2011. Slam events of high-speed catamarans in irregular waves. J. Mar. Sci. Technol. 16 (1), 8–21.

Topliss, M., Cooker, M., Peregrine, D., 1993. Pressure oscillations during wave impact on vertical walls. In: Coastal Engineering 1992, pp. 1639–1650.

Toyama, Y., 1996. Flat plate approximation in the three-dimensional slamming. J. Soc. Nav. Archit. Jpn. 1996 (179), 271–279.

Truong, D.D., et al., 2021. Prediction of slamming pressure considering fluid-structure interaction. Part II: derivation of empirical formulations. Mar. Struct. 75, 102700.

Truong, D.D., et al., 2022. Prediction of slamming pressure considering fluid-structure interaction. Part I: numerical simulations. Ships Offshore Struct. 17 (1), 7–28.

Veen, D., Gourlay, T., 2012. A combined strip theory and Smoothed Particle Hydrodynamics approach for estimating slamming loads on a ship in head seas. Ocean Eng. 43, 64–71.

Versteeg, H.K., Malalasekera, W., 2007. An Introduction to Computational Fluid Dynamics: the Finite Volume Method. Pearson education.

Von Karman, T., 1929. The Impact on Seaplane Floats during Landing.

Wagner, H., 1932. The Phenomena of Impact and Planing on Water, vol. 12. National Advisory Committee for Aeronautics Translation 1366, ZAMM, pp. 193–215.

Wang, S., Soares, C.G., 2013. Slam induced loads on bow-flared sections with various roll angles. Ocean Eng. 67, 45–57.

Wang, S., Xiang, G., Soares, C.G., 2021. Assessment of three-dimensional effects on slamming load predictions using OpenFoam. Appl. Ocean Res. 112, 102646.

Wendt, J.F., 2008. Computational Fluid Dynamics: an Introduction. Springer Science & Business Media.

Whelan, J.R., 2004. Wetdeck Slamming of High-Speed Catamarans with a Centre Bow. University of Tasmania.

Wu, G., Sun, H., He, Y., 2004. Numerical simulation and experimental study of water entry of a wedge in free fall motion. J. Fluid Struct. 19 (3), 277–289.

Xie, H., et al., 2020. Numerical study on the dynamic response of a truncated ship-hull structure under asymmetrical slamming. Mar. Struct. 72, 102767.

Xu, G., Duan, W., Wu, G., 2008. Numerical simulation of oblique water entry of an asymmetrical wedge. Ocean Eng. 35 (16), 1597–1603.

Yamada, Y., Takami, T., Oka, M., 2012. Numerical study on the slamming impact of wedge shaped obstacles considering fluid-structure interaction (FSI). In: The Twenty-Second International Offshore and Polar Engineering Conference. OnePetro.

Zhang, W., et al., 2018. URANS prediction of the slamming coefficients for perforated plates during water entry. Int. J. Marit. Eng. 160 (A1).

Zhao, R., Faltinsen, O., Aarsnes, J., 1996. In: Water Entry of Arbitrary Two-Dimensional Sections with and without Flow Separation. Proceedings of the 21st symposium on naval hydrodynamics.

Zhu, L., Faulkner, D., 1995. Design pressure for the wet-deck structure of twin-hull ships. In: Kruppa, C.F.L. (Ed.), 3rd Intl Conf on Fast Sea Transportation. Schiffbautechnische Gesellschaft: Lubeck-Travemunde, Germany.

Zong, Z., et al., 2020. Evolution of slamming load and flow field in water-entry process of trimaran ship section. Ocean Eng. 205, 107319.